

Secondary Organic Aerosol Formation and Composition from the Photo-oxidation of Methyl Chavicol (Estragole)

K. L. Pereira¹, J. F. Hamilton^{1}, A. R. Rickard^{1,2}, W. J. Bloss³, M. S. Alam³, M. Camredon⁴,
A. Muñoz⁵, M. Vázquez⁵, E. Borrás⁵, M. Ródenas⁵*

¹Wolfson Atmospheric Chemistry Laboratory, Department of Chemistry, University of York,
York, UK. ²National Centre for Atmospheric Science, University of York, UK. ³School of
Geography, Earth & Environmental Sciences, University of Birmingham, Birmingham, UK.
⁴LISA, UMR CNRS/INSU 7583, University of Paris-Est Créteil, Paris, France. ⁵CEAM-
UMH, EUPHORE, Valencia, Spain.

* Corresponding author; e-mail: jacqui.hamilton@york.ac.uk, Phone: +44 (0) 1904 324076,
Fax: +44 (0) 1904 322516

Keywords; methyl chavicol, estragole, oil palm, secondary organic aerosol, tandem mass
spectrometry.

1 **Abstract.** The increasing demand for palm oil for uses in biofuel and food products is leading
2 to rapid expansion of oil palm agriculture. Methyl chavicol (also known as estragole and 1-
3 allyl-4-methoxybenzene) is an oxygenated biogenic volatile organic compound that was
4 recently identified as the main floral emission from an oil palm plantation in Malaysian
5 Borneo. The emissions of methyl chavicol observed may impact regional atmospheric
6 chemistry, but little is known of its ability to form secondary organic aerosol (SOA). The
7 photo-oxidation of methyl chavicol was investigated at the European Photoreactor chamber
8 as a part of the atmospheric chemistry of methyl chavicol (ATMECH) project. Aerosol
9 samples were collected using a particle into liquid sampler (PILS) and analysed offline using
10 an extensive range of instruments including; high performance liquid chromatography mass
11 spectrometry (HPLC-ITMS), high performance liquid chromatography quadrupole time-of-
12 flight mass spectrometry (HPLC-QTOFMS) and Fourier transform ion cyclotron resonance
13 mass spectrometry (FTICR-MS). The SOA yield was determined as 18 and 29 % for an
14 initial VOC mixing ratio of 212 and 460 ppbv respectively; using a VOC:NO_x ratio of ~ 5:1.
15 In total, 59 SOA compounds were observed and the structures of 10 compounds have been
16 identified using high resolution tandem mass spectrometry. The addition of hydroxyl and/or
17 nitro functional groups to the aromatic ring appears to be an important mechanistic pathway
18 for aerosol formation. This results in the formation of compounds with both low volatility
19 and high O:C ratios, where functionalisation rather than fragmentation is mainly observed as
20 a result of the stability of the ring. The SOA species observed can be characterized as semi-
21 volatile to low volatile oxygenated organic aerosol (SVOOA and LVOOA) components and
22 therefore may be important in aerosol formation and growth.

23

24

25 **1. Introduction.** The atmospheric oxidation of volatile organic compounds (VOCs) in the
26 presence of NO_x results in the formation of tropospheric ozone and secondary organic aerosol
27 (SOA). Whilst SOA formation is known to have adverse effects on climate and human health
28 (Solomon et al., 2007; Bernstein et al., 2004; Davidson et al., 2005; Pöschl, 2005), the VOC
29 oxidation pathways leading to SOA formation are poorly understood (Hallquist et al., 2009).
30 It has been estimated that as many as 10⁴ - 10⁵ VOCs have been detected in the atmosphere,
31 all of which may undergo atmospheric oxidation and contribute to SOA formation (Goldstein
32 and Galbally, 2007). Approximately 90% of all global VOC emissions are from biogenic
33 sources (Guenther et al., 1995). The most abundant biogenic emissions are attributed to
34 isoprene (35-40 %), monoterpenes (11-25 %) and oxygenated VOCs (reactive other VOCs
35 and other VOCs, 20-30%) (Guenther et al., 2000; Guenther et al., 1995). The largest source
36 of biogenic VOC emissions are from vegetation; including trees (which account for ~ 71 %
37 of emissions (Guenther et al., 1995), shrubs and crops, with a small emission source from
38 grasslands and soils (Guenther et al., 1995; Zimmerman, 1979; Wiedinmyer et al., 2004;
39 Guenther et al., 2000). Oxygenated VOCs (OVOCs) have received more attention recently
40 due to the advances in instrumentation to detect and quantify these compounds in the ambient
41 atmosphere. Despite this, significant uncertainties still remain in our knowledge of the
42 sources, chemical composition and atmospheric oxidation mechanisms of OVOCs, in
43 particular higher molecular weight species (> C₅) (Singh et al., 2000; Steiner et al., 2008;
44 Taipale et al., 2012; Schade and Goldstein, 2001; Bouvier-Brown, 2008).

45

46 Methyl chavicol (C₁₀H₁₂O), also known as estragole and 1-allyl-4-methoxybenzene, is a C₁₀
47 aromatic biogenic OVOC emitted from a variety of pine trees (including *ponderosa pine*),
48 shrubs (*clausena dunniana*, *stragglely baeckea*) and common herbs (*basil*, *fennel*, *tarragon*)
49 (Werker et al., 1994; Simon et al., 1990; Southwell et al., 2003; Mirov, 1961; Bouvier-Brown

50 et al., 2009; De Vincenzi et al., 2000; Barazani et al., 2002; Adams, 2007; Holzinger et al.,
51 2010; Holzinger et al., 2005). A recent publication identified significant methyl chavicol
52 emissions above the canopy of an oil palm plantation in Malaysian Borneo, with a mean
53 midday flux of $0.81 \text{ mg m}^{-2} \text{ h}^{-1}$ and a mean mixing ratio of 3.0 ppbv (maximum mixing ratio
54 observed ~ 7.0 ppbv) (Misztal et al., 2010). Methyl chavicol emissions from palm oil
55 plantations were estimated to result in a global emission of $\sim 0.5 \text{ Tg y}^{-1}$ (Misztal et al., 2010).
56 There are currently 43 oil palm producing countries, with the majority of oil palm plantations
57 concentrated in Indonesia and Malaysia (FAOSTAT, 2012). In 2011, there were
58 approximately 7.7 million hectares (Mha) of oil palm plantations in Indonesia (USDA, 2013)
59 and 5.0 Mha in Malaysia (MPOB, 2012). The increasing demand for palm oil for uses in food
60 products and biofuels is resulting in the rapid expansion of oil palm agriculture (Fitzherbert et
61 al., 2008). Consequently, methyl chavicol emissions are likely to have a considerable effect
62 on regional chemistry in locations where oil palm plantations are significant. Despite this,
63 there have been few literature reports which have investigated the atmospheric fate of methyl
64 chavicol, including gas-phase degradation, SOA formation, composition and yields.

65

66 The gas phase products formed from the oxidation of methyl chavicol with hydroxyl radicals
67 (OH), and ozone (O_3) has been investigated by Lee et al. (2006a); Lee et al. (2006b), and
68 more recently by Bloss et al. (2012), who reported measurements of the gas-phase reactivity
69 of methyl chavicol with OH and O_3 , and by Gai et al. (2013) who in addition investigated the
70 oxidation of methyl chavicol with NO_3 . In the study performed by Lee et al., (2006b) the
71 photo-oxidation of methyl chavicol resulted in significant SOA formation (yield 40 %) and
72 the formation of two abundant structurally unidentified gas phase compounds, MW 136
73 ($\text{C}_8\text{H}_8\text{O}_2$, yield 42 ± 9 %) and MW 150 ($\text{C}_9\text{H}_{10}\text{O}_2$, yield 23 ± 5 %), detected using proton
74 transfer reaction mass spectrometry (PTR-MS). Bouvier-Brown et al. (2009) identified MW

75 136 as 4-methoxybenzaldehyde in the aerosol phase at Blodgett forest (California, US) and
76 suggested the identification of pinonaldehyde (MW 150) (Holzinger et al., 2005) could be in
77 part attributed to 4-methoxybenzene acetaldehyde (MW 150) identified in Lee et al. (2006b).
78 In addition, Cahill et al. (2006) tentatively identified 4-methoxybenzene acetaldehyde in
79 aerosol samples collected in the Sierra Nevada Mountains. More recently, Gai et al. (2013)
80 identified a further two abundant gas phase products, MW 122 4-methoxytoluene, and MW
81 166 4-methoxybenzoic acid, and identified MW 136 and MW 150 as 4-
82 methoxybenzaldehyde and 4-methoxybenzene acetaldehyde, respectively, in support of the
83 literature. To our knowledge, however, the aerosol phase composition and mechanisms of
84 formation from the photo-oxidation of methyl chavicol has largely been unexplored.

85

86 The aim of this study is to characterize the SOA oxidation products formed from the photo-
87 oxidation of methyl chavicol and determine their formation mechanisms. Experiments were
88 performed at the European Photoreactor chamber in Valencia, Spain, as a part of the
89 atmospheric chemistry of methyl chavicol (ATMECH) project. Aerosol samples were
90 collected using a particle into liquid sampler (PILS). SOA composition was investigated
91 using an extensive range of instruments, including; high performance liquid chromatography
92 ion trap mass spectrometry (HPLC-ITMS), high performance liquid chromatography
93 quadrupole time-of-flight mass spectrometry (HPLC-QTOFMS) and Fourier transform ion
94 cyclotron resonance mass spectrometry (FTICR-MS).

95

96 **2. Materials and methods**

97 **2.1 Chamber simulation experiments.** Experiments were performed at the European
98 Photoreactor (EUPHORE) in Valencia, Spain. The EUPHORE facility comprises of two 200
99 m³ hemispheric reaction chambers made of fluorinated ethyl propylene foil, with housings

100 which may be closed to exclude sunlight. Chamber temperature is near ambient and chamber
101 pressure is maintained at approximately 100 Pa above ambient. Dry scrubbed air is used
102 within the chamber and two large fans ensure homogenous mixing. Further technical
103 information regarding the chamber design and installation can be found in the literature
104 (Becker, 1996; Klotz et al., 1998; Volkamer et al., 2001; Bloss et al., 2005). A series of
105 experiments were performed during May 2012 and the initial mixing ratios, chamber
106 temperatures and relative humidities are presented in Table 1.

107

108 The chamber was cleaned before each experiment by flushing with scrubbed dry air
109 overnight. Methyl chavicol was introduced into the chamber through a heated air stream.
110 “Classical” photo-oxidation experiments were performed, where no additional $\cdot\text{OH}$ source
111 was added into the chamber. The initial source of $\cdot\text{OH}$ in these experiments was from the
112 photolysis of HONO, formed from the heterogeneous reaction of NO_2 and H_2O on the
113 chamber walls (cf. (Sakamaki et al., 1983; Pitts et al., 1984; Svensson et al., 1987; Carter et
114 al., 1981, 1982)). An extensive range of monitors were used to measure chamber temperature
115 (temperature sensor, model PT100), pressure (Barometer, model AIR-DB-VOC), humidity
116 (Hygrometer Watz, model Walz-TS2), solar intensity (J_{NO_2} Filter Radiometer), ozone
117 (Monitor Labs, model 9810) and NO_x (Teledyne API, model $\text{NO}_x\text{-API-T200UP}$; photolytic
118 converter). PTR-MS (Ionikon Analytik) and Fourier transform infra red (FTIR Nicolet
119 Magna, model 550), coupled to a white-type mirror system with an optical path length of 616
120 m, were used to monitor methyl chavicol decay and product formation. The chamber dilution
121 rate was calculated by measuring the decay of an inert tracer gas, sulphur hexafluoride (SF_6),
122 using FTIR; typical pseudo-first-order rate constants of $2 \times 10^{-5} \text{ s}^{-1}$ were obtained,
123 corresponding to a dilution lifetime around 14 hours. The formation and evolution of
124 secondary organic aerosol (SOA) was measured using a scanning mobility particle sizer (TSI

125 Incorporated, model 3080) consisting of a differential mobility analyzer (model 3081) and a
126 condensation particle counter (model 3775).

127

128 **2.2 Aerosol sampling & sample preparation.**

129 A Brechtel Manufacturing Inc (California, US) model 4002 PILS was used for aerosol
130 collection. The PILS inlet was connected to the chamber outlet using approximately 1.5
131 meters of ¼” stainless steel tubing. Aerosol samples were collected using a PM₁ impactor,
132 with an average flow rate of 13 L min⁻¹. Acidic, basic and organic gases were removed from
133 the sampled air through the use of denuders, prepared as per manufacture instructions. The
134 wash flow rate was set at 240 µL min⁻¹ and consisted of optima LC-MS grade water (Fisher
135 Scientific, UK). The sample flow rate transferred the aerosol water mixture (optima LC-MS
136 grade water) into sealed vials at a flow rate of 200 µL min⁻¹ for 30 minutes per sample.
137 Samples were collected before the addition of methyl chavicol or NO into the chamber and
138 continued sampling until after the chamber was closed. After sample collection, punctured
139 vial caps were replaced and securely sealed with parafilm. All vials were wrapped in foil to
140 minimise potential degradation from photolysis and were stored at -20 °C until analysis.
141 Collected PILS samples were evaporated to dryness using a V10 vacuum solvent evaporator
142 (Biotage, USA) and redissolved in 300 µL of 50:50 methanol:water (optima LC-MS grade,
143 Fisher, UK), with the exception of experiment MC_{high}, which was redissolved in 500 µL.

144

145 The PILS dilutes the sampled aerosol through the transfer of grown particles from the quartz
146 impactor plate into sealed vials, condensation of steam and water uptake during particle
147 growth; see Orsini et al. (2003) for further information. The sample dilution amount is
148 usually determined by spiking a known concentration of lithium fluoride into the sample
149 flow. However, no internal standard was used due to the potential effects on the analytical

150 method (e.g. adduct formation, ion suppression) and SOA composition. PILS samples were
151 evaporated to dryness to eliminate the unknown sample dilution amount. The re-suspension
152 of samples into a smaller volume, concentrated the aerosol compounds, almost certainly
153 allowing more SOA species to be observed. The re-suspension of the PILS samples into
154 50:50 methanol:water was performed to be more compatible with the high performance liquid
155 chromatography (HPLC) mobile phase and to increase the electrospray ionisation (ESI)
156 efficiency (cf. (Kearle and Verkerk, 2009)). The PILS collection efficiency has previously
157 been determined, where no appreciable loss has been found for the particle diameter range
158 investigated (30 nm to 1 μm) (Orsini et al., 2003).

159

160 **2.3 HPLC-ITMS.** SOA composition was investigated using an Agilent 1100 series HPLC
161 (Berkshire, UK) coupled to a HTC Plus ion trap mass spectrometer (IT-MS, Bruker
162 Daltonics, Bremen, Germany). A reversed phase Pinnacle C18 150 mm x 4.6 mm, 5 μm
163 particle size column (Thames Resteck, UK) was used. The HPLC mobile phase composition
164 consisted of (A) water (optima LC-MS grade, Fisher, UK) with 0.1 % formic acid (Sigma
165 Aldrich, UK) and (B) methanol (optima LC-MS grade, Fisher, UK). Gradient elution was
166 used, starting at 90 % (A) 10 % (B), moving to 0 % (A) 100 % (B) over 60 minutes, returning
167 to the initial starting conditions at 65 minutes. A 5 minute pre-run consisting of the starting
168 mobile phase composition was performed before each sample injection. The flow rate was set
169 at 0.6 mL min⁻¹ with a sample injection volume of 60 μL . ESI was used, with a dry gas flow
170 rate of 12 L min⁻¹, a dry gas temperature of 365 °C and nebuliser gas pressure of 70 psi
171 (oxygen free nitrogen, OFN, BOC, UK). The MS was operated in alternating polarity mode,
172 scanning from m/z 50 to 600. Tandem MS was achieved through the automated MS² function
173 within the Esquire software (Bruker Daltonics, software version 5.2).

174

175 **2.4 FTICR-MS.** A solariX Fourier transform ion cyclotron resonance mass spectrometer
176 with a 9.4-T superconducting magnet (Bruker Daltonics, Coventry, UK) was used and
177 externally calibrated using L-Arginine (Sigma Aldrich, UK, purity 98 %). Samples were
178 introduced into the ESI source through direct infusion, using a Hamilton 50 μL syringe
179 (Hamilton, Switzerland) at a flow rate of $120 \mu\text{L min}^{-1}$. Spectra were acquired in both
180 positive and negative ionisation modes over a scan range of m/z 50 – 800. The ESI
181 parameters were set to a dry gas flow rate of 3.7 L min^{-1} , dry gas temperature of $220 \text{ }^\circ\text{C}$, and
182 a nebulizer gas pressure of 1.2 bar (nitrogen, BOC, UK). Broadband detection mode was
183 used, with 64 spectra averages obtained for each spectrum. Ion accumulation in the ICR cell
184 was set to 0.5 seconds with a source accumulation time of 0.002 seconds. The collision RF
185 and ion cooler time was set to favour lower masses at 1300 Vpp and 0.010 seconds,
186 respectively. An approximate resolution of 38,000 at m/z 400 was obtained for both
187 ionisation modes. The spectral analysis was performed using DataAnalysis 4.0 software
188 (Bruker Daltonics, Bremen, Germany). Monoisotopic elemental formulae were calculated
189 using the following restrictions; unlimited C, H and O were allowed and up to 3 N atoms,
190 $\text{O:C} < 3$, $\text{H:C} > 0.5$, $\text{DBE} < 20$, and in positive mode, Na and K adducts were also allowed.
191 The accuracy of the molecular formulae (elemental composition) assignment is shown by the
192 error; where the error equals the difference between the exact and measured mass for the
193 assigned molecular formula. The mass error (also referred to as mass accuracy) is displayed
194 in ppm and is calculated by dividing the mass error by the exact mass for the assigned
195 molecular formula and multiplying by 10^6 . The molecular formula score refers to the fit of
196 the theoretical and measured isotopic distribution and abundance for the assigned molecular
197 formula, and is displayed in percentage. The molecular formula score is not calculated for a
198 signal to noise (S/N) ratio below 5. The combination of a high score and low mass accuracy
199 will result in few potential molecular formula assignments for a compound at a given m/z . A

200 compound with an m/z below 300, with a high score (100%) and low mass accuracy (< 5
201 ppm) results in only one potential molecular formula (Kind and Fiehn, 2006).

202

203 **2.5 HPLC-QTOFMS.** A Dionex ultimate 3000 HPLC (Thermo Scientific Inc, UK) was
204 coupled with an ultra high resolution quadrupole time-of-flight mass spectrometer (HPLC-
205 QTOFMS) (maXis 3G, Bruker Daltonics, Coventry, UK). The HPLC utilised the same
206 reverse phase Pinnacle C18 column and mobile phase composition as described in the HPLC-
207 ITMS analysis. The gradient elution runtime was shortened, starting at 90 % (A) 10 % (B),
208 moving to 0 % (A) 100 % (B) over 50 minutes and returning to the initial starting conditions
209 at 55 minutes. A 5 minute pre-run was performed before each sample injection using the
210 starting mobile phase composition. The flow rate was set to 0.6 mL min⁻¹ and the column
211 temperature controlled at 20 °C. A user defined autosampler method was created, drawing 58
212 µL of sample into the sample loop, followed by 2 µL of a 10 ppm external standard mix and
213 20 µL of 50:50 methanol:water (optima LC-MS grade, Fisher, UK). The HPLC-QTOFMS
214 was externally calibrated using ESI-L low concentration tuning mix (Agilent Technologies,
215 UK). ESI was used and the parameters were set to a dry gas flow rate of 10 L min⁻¹, dry gas
216 temperature of 350 °C and a nebulizer pressure of 4 bar (nitrogen, BOC, UK). Tandem mass
217 spectra were acquired for a mass range of m/z 50 to 800 using the auto MS² function within
218 the Compass 1.3 micrOTOF-SR3 software, control version 3.0 (Bruker Daltonics, UK). The
219 three most abundant precursor ions per spectrum were automatically selected by the software
220 and subjected to collision induced dissociation (CID). The collision energy for CID
221 fragmentation was set at 8.0 eV at a collision RF of 800.0 Vpp. The spectral analysis was
222 performed using DataAnalysis 4.0 software (Bruker Daltonics, Bremen, Germany). The
223 molecular formula error and score was automatically calculated by the DataAnalysis software
224 using the same methods as described in the FTICR-MS analysis.

225

226 **2.6 Standards & calibrations.** A 10 ppm external standard (ES) mix was used to monitor the
227 ITMS detector variation over the course of the sample analysis. The ES mix was also used for
228 the optimisation of the HPLC-QTOFMS method, internal mass calibration and to determine
229 the retention time shift of the SOA compounds due to the shortening of the gradient elution.
230 The ES mix consisted of 5 compounds, 4-methoxybenzoic acid (Sigma Aldrich, UK, purity
231 99 %), hexanedioic acid (Sigma Aldrich, UK, purity 99 %), cis-pinonic acid (Sigma Aldrich,
232 UK, purity 99 %), 2-hydroxyhexanoic acid (Acros Organics, Belgium, purity 95 %) and 2,6-
233 dimethyl-3-nitrophenol (synthesized by University College Cork). These compounds were
234 selected based on their range of retention times, stability, variety of functional groups and
235 ionisation efficiency in both positive and negative ionisation modes. Calibrations were
236 performed using the HPLC-ITMS for any structurally identified SOA compounds where
237 standards were commercially available. Calibrations ranged in concentration from 0.02 to 2
238 ppm and consisted of a minimum of 5 concentrations, with 3 replicate measurements.

239

240 **3. Results & discussion.** Three experiments carried out as part of the ATMECH campaign
241 are discussed here: (i) MC₍₀₎; a chamber background experiment, where no VOCs or NO_x
242 were added to the chamber and the chamber housing was opened to expose the chamber to
243 light. None of the methyl chavicol SOA compounds identified were observed in this
244 experiment. (ii) MC_{high}; a photo-oxidation experiment with high initial mixing ratios of
245 methyl chavicol (460 ppbv) and NO (92 ppbv) and, (iii) MC_{low}; a photo-oxidation experiment
246 with lower mixing ratios of methyl chavicol (212 ppbv) and NO (38 ppbv), with a similar
247 initial VOC:NO_x ratio (~5:1) to MC_{high}. The VOC:NO_x ratio represents the lower MC:NO_x
248 ratio of an agro-industrialized oil palm plantation site in northern Borneo (Hewitt et al., 2009;
249 MacKenzie et al., 2011); where the boundary layer (500-800 m) NO_x concentration (75th

250 percentile) was ~ 0.6 ppbv (Hewitt et al., 2009), with a methyl chavicol abundance of ~ 3
251 ppbv at midday (MacKenzie et al., 2011), corresponding to a MC/NO_x ratio of 5. The
252 temporal evolution of NO_x, O₃, methyl chavicol and SOA growth are shown in Figure 1 and
253 show similar profiles to previous aromatic photo-oxidation experiments, with initiation of
254 aerosol formation occurring when the photo-chemical system enters into a relatively “low
255 NO” state (cf. (Rickard et al., 2010)). The maximum SOA mass observed, corrected for wall
256 loss and chamber dilution, was $420 \mu\text{g m}^{-3}$ and $126 \mu\text{g m}^{-3}$ in MC_{high} and MC_{low}, respectively.
257 The SOA yield (Y) was calculated using the equation given in Odum et al. (1996), where the
258 amount of aerosol mass formed [$\Delta M_0, \mu\text{g m}^{-3}$] was divided by the amount of methyl chavicol
259 reacted [$\Delta\text{MC}, \mu\text{g m}^{-3}$], assuming spherical aerosol shape with a density of 1.4 g cm^{-3} . The
260 SOA yield was determined as 18 % and 29 % for experiments MC_{low} and MC_{high},
261 respectively, showing a larger yield at higher initial mixing ratios as seen previously (Song et
262 al., 2005; Odum et al., 1996; Pankow, 1994a, b).

263

264 **3.1 SOA composition.** The PILS samples were analysed using a series of complementary
265 analytical techniques. Initially, the HPLC-ITMS was used to screen the PILS samples for
266 SOA species. Any compounds observed in the PILS samples before the introduction of
267 methyl chavicol and NO into the chamber in MC_{high} and MC_{low} were excluded from further
268 analysis. Compounds which displayed changes in their chromatographic peak areas (and thus
269 concentration) were investigated further. In the MC_{high} experiment, 59 SOA compounds were
270 observed in the PILS samples using HPLC-ITMS. Of these compounds, 56 were observed
271 with matching retention times and/or fragmentation patterns in the MC_{low} experiment. Three
272 compounds at a MW of 214, 226 and 250 g mol^{-1} were not observed in the lower
273 concentration experiment, MC_{low}. In MC_{high}, the intensities of these compounds in the HPLC-
274 ITMS analysis were observed just above the limit of detection (defined as $3 \times \text{S/N}$). The

275 similarity of the oxidation products formed, but the lower initial mixing ratio in MC_{low} ,
276 suggests these compounds were not observed in the MC_{low} experiment due to a decrease in
277 the formation yields at lower initial mixing ratios and/or decrease in the gas-particle
278 absorption due to the smaller amount of aerosol mass formed (Pankow, 1994a, b; Odum et
279 al., 1996; Kroll and Seinfeld, 2008). In MC_{high} , fragmentation data was obtained for 56 of the
280 59 SOA compounds using HPLC-ITMS². In many cases it was not possible to identify the
281 compound structures of the SOA species due to the low mass resolution of the ITMS and lack
282 of commercially available standards. This resulted in the use of the FTICR-MS to aid in the
283 identification of the SOA molecular formulae and compound structures. The use of FTICR-
284 MS significantly aided in compound identification, providing the molecular formulae for 49
285 of the 59 SOA compounds with average error of 0.89 ppm for negative ionisation mode and
286 4.75 ppm for positive ionisation mode. FTICR-MS² could not be performed due to the lack of
287 prior chromatographic separation and the low concentration of the SOA compounds. Instead,
288 HPLC-QTOFMS² was used to obtain high mass resolution compound fragmentation data for
289 the SOA compounds. The HPLC-QTOFMS identified the molecular formulae of 55 of the 59
290 SOA compounds with an average error of 4.13 ppm for negative ionisation mode and 18.34
291 ppm for positive ionisation mode. The use of the HPLC-QTOFMS was complementary to the
292 FTICR-MS, allowing the comparison of two high mass resolution data sets to determine the
293 molecular formulae of the SOA compounds, as shown in Table 2 and SI Table 1 & 2. The use
294 of prior chromatographic separation with the QTOFMS was advantageous and allowed the
295 molecular formulae of the 10 low concentration SOA compounds not identified using
296 FTICR-MS to be determined. Of the 59 SOA compounds, the FTICR-MS and the HPLC-
297 QTOFMS were in agreement of the molecular formulae for 40 SOA compounds. Only one
298 high resolution mass spectrometric technique provided the molecular formulae for 14 SOA
299 compounds and for 5 SOA compounds the molecular formulae provided by the HPLC-

300 QTOFMS and FTICR-MS were not in agreement. A complete list of the identified SOA
301 species including the molecular formulae identification and associated errors can be found in
302 the supplementary information, SI Tables 1 and 2.

303

304 A Van Krevelen plot of the 59 SOA compounds is shown in SI Figure 1. The average O:C
305 and H:C ratio was determined as 0.46 and 1.37, respectively. Of the 59 SOA compounds, the
306 structures of 10 have been assigned and are shown in Table 2. The structures of (4-
307 methoxyphenyl)acetic acid and 4-methoxybenzoic acid have been confirmed using the
308 retention time and fragmentation patterns of commercially available standards. All other
309 compound structures have been determined from the deprotonated or protonated molecular
310 species fragmentations obtained from the HPLC-ITMS² and HPLC-QTOFMS². Calibrations
311 were performed for 4-methoxybenzoic acid and (4-methoxyphenyl)acetic using the
312 commercially available standards. Detector variation during sample analysis was determined
313 for both compounds by measuring the peak area of 4-methoxybenzoic acid in the 10 ppm ES
314 mix. A 6 % standard deviation is shown and includes a detector variation of 5.14 % (based on
315 4 replicate measurements) plus a negligible amount for the PILS collection efficiency (see 2.2
316 Aerosol sampling & sample preparation). The concentration of 4-methoxybenzoic acid and
317 (4-methoxyphenyl)acetic acid in MC_{high} was determined as 1.26 ± 0.08 and $0.41 \pm 0.02 \mu\text{g m}^{-3}$;
318 ³; representing a total percentage SOA mass of 0.44 ± 0.03 and 0.14 ± 0.01 %, respectively.
319 In MC_{low}, the concentration of 4-methoxybenzoic acid was determined as $0.23 \pm 0.01 \mu\text{g m}^{-3}$,
320 corresponding to a percentage SOA mass of 0.26 ± 0.02 %. The HPLC-ITMS intensity of (4-
321 methoxyphenyl)acetic acid in the MC_{low} experiment was observed below the limit of
322 quantification (defined as 5 x S/N) and thus the concentration and total percentage SOA mass
323 for this compound could not be determined.

324

325 The product ions of two deprotonated molecular species are discussed here as examples to
326 illustrate the methodology used to assign SOA compound structures. Compound 1 with a
327 MW of 243 g mol⁻¹ was assigned the molecular formula C₁₀H₁₃NO₆ with 5 double bond
328 equivalents (Khan et al.). Compound 1 contains the same number of carbon atoms and one
329 more degree of saturation than the original VOC precursor, methyl chavicol (C₁₀H₁₂O). In
330 addition, compound 1 was identified in the first PILS sample containing SOA (shortest
331 reaction time, between 41 to 71 minutes into MC_{high}) in the MC_{high} experiment. The similarity
332 of the carbon number, degree of saturation, and the identification of this compound during the
333 initial particle growth, would suggest the structure of compound 1 was similar to that of the
334 precursor, a substituted methoxyphenyl. The product ions of *m/z* 242 [M-H]⁻ (compound 1)
335 are summarized in Table 3. Compound 1 was identified as 3-(5-hydroxy-4-methoxy-2-
336 nitrophenyl)propane-1,2-diol using the observed fragments discussed below and shown in
337 Figure 2. The highest intensity fragment ion at *m/z* 224 is due to the loss of water (H₂O)
338 occurring through hydrogen abstraction, Figure 2A. The base peak loss of H₂O would suggest
339 the presence of an aliphatic alcohol, most likely terminal. The loss of H₂O results in an
340 intermolecular rearrangement of the fragment ion, resulting in the formation of a double
341 bond, indicated by the increase in the DBE by 1. The fragment ion at *m/z* 182 has formed as a
342 result of a subsequent loss of C₂H₂O from *m/z* 224, which is supported by the decrease in the
343 DBE by 1 for the remaining fragment ion. The fragment ion at *m/z* 182 results from a total
344 loss of C₂H₄O₂, suggesting the presence of a second hydroxyl group on the leaving group,
345 most likely on the adjacent carbon to the first alcohol group, Figure 2B. The fragment ion at
346 *m/z* 167 has formed as a result of an odd electron cleavage (OE), resulting in the formation of
347 [C₇H₅NO₄]^{-•} and the loss of [C₃H₇O₂][•], Figure 2C. OE cleavages are unusual in CID and are
348 often associated with resonance stabilised ring structures and nitrogen containing functional
349 groups (Fu et al., 2006; Holčapek et al., 2010; Hayen et al., 2002; Holčapek et al., 2007).

350

351 Assuming the remaining deprotonated radical fragment ion at m/z 167 $[\text{C}_7\text{H}_5\text{NO}_4]^{-\bullet}$ is a
352 substituted methoxyphenyl, the subtraction of the methoxy $[\text{OCH}_3]$ and aromatic $[\text{C}_6\text{H}_2]$
353 group from the molecular formula would leave N_1O_3 unaccounted for. This suggests either a
354 nitrate group (R-ONO_2), or a hydroxyl (R-OH) and a nitro (R-NO_2) group are attached to the
355 ring. The presence of a nitrate group on the ring is likely to result in the loss of NO_2 or ONO_2
356 from the fragmentation of the carbon-oxygen or oxygen-nitrogen bond during CID (Zhao and
357 Yinon, 2002; Holčapek et al., 2010). Furthermore, the lability of the nitrate group often
358 results in spontaneous fragmentation in the softest ESI conditions, resulting in the fragment
359 ions ONO_2 and NO_2 at m/z 63 and m/z 47, respectively (Holčapek et al., 2010; Yinon et al.,
360 1997). However, no fragment ion at m/z 63 for ONO_2 was observed. A peak at m/z 137
361 (intensity 1.33%) was observed and was attributed to $[\text{C}_7\text{H}_5\text{O}_3]^{-\bullet}$, the loss of NO from the
362 fragment ion at m/z 167 $[\text{C}_7\text{H}_5\text{NO}_4]^{-\bullet}$, Figure 2C. The loss of NO is a typical for nitro
363 functional groups in negative ionisation mode using CID (Holčapek et al., 2010; Fu et al.,
364 2006; Schmidt et al., 2006; Yinon et al., 1997). The rearrangement of bonds from R-NO_2 to
365 R-ONO results in the loss of NO (Schmidt et al., 2006). Nitro functional groups usually result
366 in the loss of NO and NO_2 . However, the loss of only NO has been observed for some
367 compounds containing a nitro functional group and has previously been suggested to be the
368 result of an electron donating substituent in the para position to the nitro group, enhancing the
369 loss of NO by resonance stabilisation (Burseley and McLafferty, 1966; Burseley, 1969).

370

371 The location of phenyl substitutions has proved to be difficult to determine using CID due to
372 the lack of ring fragmentation as a result of resonance stabilisation. In addition, the N-
373 containing compounds that were observed to undergo ring fragmentation exhibited complex

374 re-arrangements making the identification of these compound structures a difficult task. The
375 most likely locations of phenyl substitutions can be identified however, by considering the
376 formation mechanisms of these compounds in the gas phase (Ziemann and Atkinson, 2012;
377 Calvert et al., 2002). Methyl chavicol has two phenyl substituents, a methoxy group and an
378 hydrocarbon (HC) chain, both of which are ortho, para directing (March, 1992). The stronger
379 activating group of the two phenyl substituents, the methoxy group, will determine the most
380 energetically favoured and resonance stabilised position of an addition to the ring (March,
381 1992). The para position to the methoxy group is occupied by the HC chain and therefore the
382 initial oxidation of a hydroxyl radical to the ring of methyl chavicol would be most
383 energetically favoured at the ortho position to the methoxy group (Ziemann and Atkinson,
384 2012). The location of the nitro group on the ring is more difficult to assign. Assuming the
385 hydroxyl radical is already attached to the ring, the most strongly activating group would now
386 be the hydroxyl group, which is also ortho, para directing (March, 1992). The ortho position
387 to the hydroxyl group is more sterically hindered by the adjacent HC chain and hydroxyl
388 group, compared to the para position, which is only sterically hindered by the HC chain. It is
389 therefore suggested that the nitro group is located in the para position to the hydroxyl group.
390 The suggested location of the nitro and hydroxyl group on the ring is also supported by the
391 mechanism suggested in (Bursey, 1969; Bursey and McLafferty, 1966), where the loss of
392 only NO is observed for a nitro functional group during CID when an activating group is
393 located in the para position to the nitro group.

394

395 Compound 5, with a MW of 198 g mol^{-1} was assigned the molecular formula $\text{C}_{10}\text{H}_{14}\text{O}_4$ with 4
396 DBE. The product ions of m/z 197 $[\text{M}-\text{H}]^-$ (compound 5) are summarized in Table 4.
397 Compound 5 was identified as 3-(3-hydroxy-4-methoxyphenyl)propane-1,2-diol from the
398 product ions discussed here and shown in Figure 3. Both compounds 1 and 5 exhibit similar

399 HC chain fragmentation, with the loss of 18 Da (H₂O) and 42 Da (C₂H₂O₂), Figure 3A & B.
400 The product ion [C₇H₇O₂]⁻ at *m/z* 123 resulted from an even electron (EE) loss of C₃H₆O₂,
401 unlike the OE loss of [C₃H₇O₂]⁻ observed for compound 1, Figure 3C. Compound 5 does not
402 have a nitro group present on the ring and as a result the resonance stabilization of the
403 aromatic ring is lower than in compound 1. The decrease in resonance stabilisation results in
404 an EE cleavage and the abstraction of a hydrogen from the leaving group to the aromatic ring.
405 Hydrogen abstraction from the loss group results in an intermolecular re-arrangement and the
406 loss of C₃H₆O₂. Therefore, the same HC chain has been suggested for both compounds 1 and
407 5. Assuming a methoxyphenyl sub-structure, the deprotonated product ion would leave
408 [C₆H₃O]⁻ from product ion [C₇H₇O₂]⁻ at *m/z* 123, suggesting a hydroxyl group is attached to
409 the aromatic ring.

410

411 **3.2. Mechanism of formation.** A proposed mechanism for the formation of compounds 1, 5,
412 8, 9 and 10 is shown in Figures 4a and b. The formation of these compounds can be
413 rationalised as the products of methyl chavicol oxidation by considering typical gas phase
414 oxidation mechanisms (Ziemann and Atkinson, 2012; Calvert et al., 2002). The reaction rate
415 constants of methyl chavicol with [•]OH and O₃ have previously been determined as 5.20 ±
416 0.78 × 10⁻¹¹ and 1.03 ± 0.23 × 10⁻¹⁷ cm³ molecule⁻¹ s⁻¹, respectively (Gai et al., 2013). The
417 proportion of methyl chavicol reacting with [•]OH and O₃ during MC_{low} and MC_{high} is shown in
418 SI, Figures 2 and 3, respectively; where throughout both experiments the reaction of methyl
419 chavicol with [•]OH is observed to dominate over the reaction with O₃. The initial oxidation of
420 methyl chavicol will proceed mainly through the [•]OH radical addition mechanism (Atkinson,
421 1997a; Calvert et al., 2002; Ziemann and Atkinson, 2012) and can attack the ring and/or the
422 HC chain. [•]OH radical addition can occur on either carbon of the double bond of the HC
423 chain, resulting in the formation of primary and secondary β-hydroxyalkyl radicals, with the

424 secondary β -hydroxyalkyl radical pathway being the most favoured (approximately 85 %
425 using (Peeters et al., 2007) $\cdot\text{OH}$ addition structure activity relationship) (Atkinson, 2000,
426 1997a; Cvetanovic, 1976). The resulting β -hydroxyalkyl radicals react predominantly with O_2
427 to form β -hydroxyperoxy radicals. The high concentration of NO at the beginning of MC_{high}
428 and MC_{low} will result in the conversion of NO to NO_2 (leading to O_3 formation) and the
429 formation of β -hydroxyalkoxy radicals as the major pathway. β -hydroxyalkoxy radicals can
430 react with O_2 , decompose or isomerize. Decomposition and isomerisation are expected to be
431 the dominant pathways, with the exception of the $\text{HOCH}_2\text{CH}_2\text{O}\cdot$ radical (from ethene + $\cdot\text{OH}$),
432 for which decomposition and reaction with O_2 can be competitive (Atkinson, 1997a, b; Fuchs
433 et al., 2011).

434

435 For both types of β -hydroxyalkoxy radicals formed, decomposition followed by rapid
436 reaction with O_2 leads to the formation of formaldehyde, HO_2 and (4-
437 methoxyphenyl)acetaldehyde (Atkinson, 1997a; Orlando et al., 2003). Isomerisation through
438 a 1, 5-H atom shift from the aromatic ring to the HC chain is suggested to be of minor
439 importance due to the resonance stability of the ring. The reaction with O_2 (minor pathway)
440 would result in the loss of HO_2 and the formation of the observed first generation compound,
441 1-hydroxy-3-(4-methoxyphenyl)propan-2-one (compound 9), Figure 4a (A). Further
442 oxidation of this compound through the addition of a hydroxyl radical to the ring results in
443 the formation of 1-hydroxy-3-(3-hydroxy-4-methoxyphenyl)propan-2-one (compound 10),
444 Figure 4a (B). As discussed in the previous section, the initial hydroxyl addition to the ring
445 will occur at the ortho position to the methoxy group, the position which is most energetically
446 favoured and resonance stabilised. Compound 8, 2-hydroxy-3-(3-hydroxy-4-
447 methoxyphenyl)propanal, is also suggested to be a second generation compound which has
448 formed through the oxidation of the primary β -hydroxyalkoxy radicals with O_2 (the less

449 favoured pathway) and has been further oxidised by the addition of a hydroxyl radical to the
450 ring, Figure 4b (A).

451

452 As a relatively “low NO_x state” is entered in MC_{high} and MC_{low} the RO₂ + RO₂ or HO₂
453 reaction will begin to dominate over the competing reaction with NO (Atkinson, 1997a;
454 Stockwell et al., 1990). The cross/self reaction of β-hydroxyperoxy radicals will proceed
455 mainly through two pathways; the radical pathway and non-radical pathway (hydrogen
456 abstraction), with the radical pathway accounting for approximately 30 - 80 % of the RO₂ +
457 RO₂ reaction (Atkinson, 1997a; Madronich and Calvert, 1990). The radical pathway (major
458 pathway) will result in the formation of β-hydroxyalkoxy radicals with the loss of O₂. The β-
459 hydroxyalkoxy radicals can then undergo oxidation through the same mechanisms as
460 discussed above, resulting in a secondary pathway for the formation of compounds 8, 9 and
461 10, Figure 4b (B), Figure 4a (C) and (D), respectively. A third minor pathway to the
462 formation of compounds 8, 9 and 10 can also occur through the RO₂ + RO₂ non radical
463 pathway; where one peroxy radical abstracts a hydrogen atom from another peroxy radical,
464 resulting in the formation of an alcohol and carbonyl, respectively, with the loss of O₂
465 (Madronich and Calvert, 1990; Howard and Ingold, 1968). The hydrogen atom is abstracted
466 from the carbon bonded to the peroxy radical, thus the abstraction of a hydrogen atom from a
467 secondary β-hydroxyperoxy radical will result in the formation of 1-hydroxy-3-(4-
468 methoxyphenyl)propan-2-one (compound 9), Figure 4a (E). The further oxidation of this
469 compound though the reaction with •OH will result in the formation of 1-hydroxy-3-(3-
470 hydroxy-4-methoxyphenyl)propan-2-one (compound 10), Figure 4a (F). Moreover, the
471 abstraction of a hydrogen from a primary β-hydroxyperoxy radical followed by the further
472 oxidation of an •OH radical to the ring, will result in the formation of 2-hydroxy-3-(3-
473 hydroxy-4-methoxyphenyl)propanal (compound 8), Figure 4b (C).

474

475 The formation of the diol on the HC chain of compound 1 [3-(5-hydroxy-4-methoxy-2-
476 nitrophenyl)propane-1,2-diol], and compound 5 [3-(3-hydroxy-4-methoxyphenyl)propane-
477 1,2-diol], could have occurred through two mechanisms; unimolecular isomerisation of the β -
478 hydroxyalkoxy radical through a 1,5 H-atom shift, or the self/cross RO₂ reactions of the β -
479 hydroxyperoxy radicals through the non-radical pathway. The isomerisation pathway would
480 seem unlikely due to the formation of a alkyl radical on the carbon where the H-atom was
481 abstracted, which could decompose, isomerise, or react with O₂, with the latter resulting in the
482 formation of a more oxidised product than observed. Decomposition would result in the
483 formation of a compound with fewer carbon atoms than required, and isomerisation would
484 still result in an alkyl radical. The self/cross reactions of β -hydroxyperoxy radicals would
485 appear to be the more likely pathway, particularly under low NO_x conditions. After the
486 formation of a diol on the HC chain, the further oxidation *via* hydroxyl radical addition to the
487 ring would result in the formation of the third generation SOA compound, 3-(3-hydroxy-4-
488 methoxyphenyl)propane-1,2-diol (compound 5), Figures 4a (G) and Figure 4b (D). Further
489 addition of NO₂ to the ring of compound 5 through the hydrogen atom abstraction pathway
490 leads to the formation of a fourth generation SOA compound 3-(5-hydroxy-4-methoxy-2-
491 nitrophenyl)propane-1,2-diol (Compound 1), Figures 4a (H) and Figure 4b (E). A hydroxyl
492 radical can abstract a hydrogen atom from the oxygen-hydrogen bond of the hydroxyl group
493 on the substituted phenol, resulting in the formation of a phenoxy radical and the loss of H₂O
494 (Forstner et al., 1997; Atkinson, 2000; Atkinson, 1994). The phenoxy radical can then react
495 with NO₂ to form a substituted nitrophenol (Atkinson, 2000; Atkinson, 1994; Forstner et al.,
496 1997).

497

498 Compounds 2, 3, 4, 6 and 7, contain acid functional groups and less carbon atoms than the
499 original VOC precursor, methyl chavicol. These compounds appear to be later generation
500 SOA species and could have formed through a number of potential mechanisms, such as
501 reactions with ozone (O'Neal and Blumstein, 1973; Orzechowska and Paulson, 2005; Neeb et
502 al., 1996; Calvert et al., 2000), and/or with hydroxyl radicals (Forstner et al., 1997; Gai et al.,
503 2013), although the detailed reaction mechanisms for the formation of organic acids from
504 hydroxyl radicals has not been properly established (Carlton et al., 2009). Compounds 4 and
505 7 appear to be the further oxidation products of compounds 2 and 6, through the addition of a
506 hydroxyl radical to ring. In addition, compound 3 appears to be the further oxidation product
507 of compound 7, through a second addition of a hydroxyl radical to the ring. Here we suggest
508 the second addition of the hydroxyl radical to the ring of compound 7 is in the para position
509 to the hydroxyl group, the most resonance stabilised and least sterically hindered position.

510

511 **3.3 Atmospheric relevance.** The SOA yield obtained in this study for the photo-oxidation of
512 methyl chavicol, in MC_{low} (18 %) and MC_{high} (29 %) are comparatively lower than the 40 %
513 SOA yield reported previously (Lee et al., 2006b), although there are a number of key
514 difference between the two studies. Lee et al. (2006b) used ammonium sulfate seed
515 (compared to the nucleation only experiments presented here), which has been shown to
516 increase the SOA yields of aromatic precursors (Kroll et al., 2007; Huang et al., 2013; Lu et
517 al., 2009). In addition, the percentage relative humidity (% RH) was approximately 5 times
518 greater in the study performed by Lee et al. (2006b). Recent publications have shown that the
519 SOA mass formed from a substituted aromatic compound (*p*-xylene), increases with
520 increasing % RH, approximately by a factor of 2 over a % RH range of 5 to 75 % (Zhou et
521 al., 2011; Healy et al., 2009). Nevertheless, it is clear the photo-oxidation of methyl chavicol
522 results in significant SOA formation. Recent literature has shown oxygenated biogenic VOCs

523 containing 10 carbon atoms (including eucalyptol, verbenone, linalool) resulted in an SOA
524 yield between 16 to 20 %, with the use of neutral (Iinuma et al., 2008; Varutbangkul et al.,
525 2006; Lee et al., 2006b) or acidic (Iinuma et al., 2008) seed. It is difficult to directly compare
526 SOA yields from the oxidation of a similar VOC precursors in the literature due to the
527 limitations of using chamber derived data (Camredon et al., 2007). However, reported SOA
528 yields of methyl chavicol were the highest of all oxygenated VOCs investigated (SOA yield
529 26 – 40 %) (Lee et al., 2006b; Varutbangkul et al., 2006). Although these experiments are at
530 concentrations higher than the real atmosphere, they suggest that methyl chavicol can act as
531 an important SOA precursor in regions where methyl chavicol emissions are significant, such
532 as downwind from pine forests and oil palm plantations.

533

534 Aerosol loadings where methyl chavicol emissions are significant, such as northern Borneo,
535 have been found to range from $5 \mu\text{g m}^{-3}$ (800 meters above the oil palm plantation) to $100 \mu\text{g}$
536 m^{-3} (in a chimney plume of a near-source oil palm processing plant) (MacKenzie et al.,
537 2011). The aerosol loadings formed in these experiments are considerably higher (MC_{low} 126
538 and MC_{high} $430 \mu\text{g m}^{-3}$) than the aerosol loadings observed in ambient conditions. It is
539 therefore likely that more compounds are observed in the aerosol phase in this study than
540 would be at atmospherically relevant conditions; due to more higher volatility species
541 partitioning into the aerosol phase at higher mass loadings (Pankow, 1994a, b; Odum et al.,
542 1996). However, the structurally identified compounds were characterized as semi- to low-
543 volatility oxygenated organic aerosol; where at atmospherically relevant conditions a sizable
544 fraction of these compounds would be expected to exist in the aerosol phase (cf. (Donahue et
545 al., 2012)).

546

547 The SOA compounds identified in this study will be representative of methyl chavicol
548 oxidation products formed in polluted environments (high NO_x) and downwind of pollution
549 sources (low NO_x, high O₃). At the start of the chamber experiments, the high NO
550 concentrations will be representative of methyl chavicol emissions directly next to a high NO
551 source, such as a processing plant (MacKenzie et al., 2011). Here, the peroxy radicals (ROO[•])
552 will preferentially react with NO forming alkoxy radicals (RO[•]) and NO₂ (leading to O₃
553 formation). As a relatively low NO environment in the chamber is entered (i.e. the majority
554 of NO has been converted to NO₂), the RO₂ radicals will increasingly react with RO₂ or
555 (primarily) HO₂; instead of NO. The oxidation products formed whilst the NO concentration
556 is relatively low but the NO₂ concentration is near maximum, will be representative of the
557 methyl chavicol oxidation products formed in polluted environments, i.e. agro-industrialized
558 oil palm plantation site (MacKenzie et al., 2011). As the chamber experiment progresses, the
559 NO₂ concentration decreases, approaching zero (as the NO_x is not replenished in the
560 chamber) and the O₃ concentration increases from the photolysis of NO₂. This chamber
561 scenario then corresponds to an environment representative of the products formed
562 downwind of an agro-industrialized oil palm plantation; where there is less pollution (low
563 NO_x), but O₃ is present.

564

565 Four compounds with a MW of 122, 136, 150 and 166 g mol⁻¹ were observed in the gas phase
566 using PTR-MS and may be attributed to 4-methoxytoluene, 4-methoxybenzaldehyde, 4-
567 methoxybenzene acetaldehyde and (4-methoxyphenyl)acetic acid, respectively, in agreement
568 with Lee et al. (2006b), Spada et al. (2008) and Gai et al. (2013). These compounds are
569 formed as a result of decomposition leading to higher volatility species and are therefore not
570 included in Figures 4a and b. The gas phase oxidation mechanisms of these compounds can
571 be observed in Gai et al. (2013). In contrast to Cahill et al. (2006) and Bouvier-Brown et al.

572 (2009) 4-methoxybenzaldehyde (MW 136) and 4-methoxybenzene acetaldehyde (MW 150)
573 were not identified in the aerosol phase in this study. Compound vapour pressures were
574 calculated using the UManSysProp website (<http://ratty.cas.manchester.ac.uk/informatics/>) at
575 298.15 K, using the Nannoolal vapour pressure and boiling point extrapolation method
576 (Nannoolal et al., 2008; Nannoolal et al., 2004) and the saturation concentration (C^* , $\mu\text{g m}^{-3}$)
577 determined (Donahue et al., 2006a). The calculated volatility of these compounds suggests
578 they are intermediate VOCs (4-methoxybenzaldehyde, $C^* = 4.96 \times 10^5 \mu\text{g m}^{-3}$ and 4-
579 methoxybenzene acetaldehyde, $C^* = 3.02 \times 10^5 \mu\text{g m}^{-3}$). The use of gas phase scrubbers for
580 organics in the PILS sampler used in this study may indicate that previous ambient
581 observations are due to positive artifacts from gas phase absorption to filters.

582

583 The saturation concentration (C^* , $\mu\text{g m}^{-3}$) (Donahue et al., 2006a) and O:C ratio were
584 determined for all the identified compounds and plotted in a O:C /log C^* , $\mu\text{g m}^{-3}$ volatility
585 basis set space (Donahue et al., 2013; Jimenez et al., 2009), as shown in Figure 5. All of the
586 identified SOA compounds retained the aromatic ring, with O:C ratios between 0.30 to 0.63
587 and H:C ratios between 1.00 and 1.40. The oxidation of methyl chavicol and its early
588 generation products resulted in the formation of low vapour pressure and a high O:C ratio
589 species, due to the lack of ring fragmentation. This resulted in the movement of the SOA
590 compounds to lower volatilities and higher O:C ratios, thus functionalisation rather than
591 fragmentation was mainly observed. The majority of the structurally identified SOA species
592 underwent oxidation on the aromatic ring, through the addition of $\cdot\text{OH}$ and/or NO_2 . The
593 formation of compound 1 (3-(5-hydroxy-4-methoxy-2-nitrophenyl)propane-1,2-diol) through
594 the addition of a NO_2 group on the aromatic ring resulted in the movement of this species to
595 the low volatility oxygenated organic aerosol region (LVOOA), and just outside the
596 extremely low volatility oxygenated organic aerosol (ELVOOA) nucleator region proposed

597 by Donahue et al. (2013). Ring addition appears to be an important pathway, resulting in the
598 formation of low volatility species with high O:C ratios, which may also be important for
599 other aromatic compounds. Only structures for 8 of the 59 compounds detected could be
600 tentatively identified; however, 2 structures were confirmed with authentic standards. Further
601 work is required to characterize the SOA formed from methyl chavicol oxidation at different
602 mixing ratios and with different oxidants (O_3 , NO_3), NO_x levels, RHs and seed aerosol
603 compositions.

604

605 **Acknowledgements.** The assistance of scientists at EUPHORE and the York Centre of
606 Excellence in Mass Spectrometry is gratefully acknowledged. This work was supported by
607 EUROCHAMP-2 (TA Project E2-2011-04-19-0059). ARR acknowledges the support of
608 the National Centre for Atmospheric Science. The York Centre of Excellence in Mass
609 Spectrometry was created thanks to a major capital investment through Science City York,
610 supported by Yorkshire Forward with funds from the Northern Way Initiative. KEP
611 acknowledges support of a NERC PhD studentship (NE106026057).

References.

Adams, R. P.: Identification of essential oil components by gas chromatography/mass spectrometry, Ed. 4, Allured Publishing Corporation, Carol Stream, 2007.

Atkinson, R.: Gas-phase tropospheric chemistry of organic compounds., Journal of Physical and Chemical Reference Data, Monograph, 2, 1-216, 1994.

Atkinson, R.: Gas-phase tropospheric chemistry of volatile organic compounds .1. Alkanes and alkenes, J Phys Chem Ref Data, 26, 215-290, 1997a.

Atkinson, R.: Atmospheric reactions of alkoxy and beta-hydroxyalkoxy radicals, *Int J Chem Kinet*, 29, 99-111, Doi 10.1002/(Sici)1097-4601(1997)29:2<99::Aid-Kin3>3.0.Co;2-F, 1997b.

Atkinson, R.: Atmospheric chemistry of VOCs and NO_x, *Atmospheric Environment*, 34, 2063-2101, Doi 10.1016/S1352-2310(99)00460-4, 2000.

Barazani, O., Cohen, Y., Fait, A., Diminshtein, S., Dudai, N., Ravid, U., Putievsky, E., and Friedman, J.: Chemotypic differentiation in indigenous populations of *Foeniculum vulgare* var. *vulgare* in Israel, *Biochem Syst Ecol*, 30, 721-731, Pii S0305-1978(02)00019-4 Doi 10.1016/S0305-1978(02)00019-4, 2002.

Becker, K.: EUPHORE: Final report to the European commission, Contract# EV5V-CT92-0059, Bergische Universität Wuppertal, Germany, 1996.

Bernstein, J. A., Alexis, N., Barnes, C., Bernstein, I. L., Bernstein, J. A., Nel, A., Peden, D., Diaz-Sanchez, D., Tarlo, S. M., and Williams, P. B.: Health effects of air pollution, *The Journal of allergy and clinical immunology*, 114, 1116-1123, 10.1016/j.jaci.2004.08.030, 2004.

Bloss, C., Wagner, V., Bonzanini, A., Jenkin, M. E., Wirtz, K., Martin-Reviejo, M., and Pilling, M. J.: Evaluation of detailed aromatic mechanisms (MCMv3 and MCMv3.1) against environmental chamber data, *Atmos. Chem. Phys.*, 5, 623-639, 10.5194/acp-5-623-2005, 2005.

Bloss, W. J., Alam, M. S., Rickard, A. R., Hamilton, J. F., Pereira, K. L., Camredon, M., Muñoz, A., Vázquez, M., Alacreu, P., Ródenas, M., and Vera, T.: Atmospheric Chemistry of Methyl Chavicol (Estragole), AGU Fall Meeting, San Francisco, Fall meeting 3 to 7 December 2012, A33L-0313, 2012.

Bouvier-Brown, N., Goldstein, A., Worton, D., Matross, D., Gilman, J., Kuster, W., Welsh-Bon, D., Warneke, C., de Gouw, J., and Cahill, M.: Methyl chavicol: characterization of its

biogenic emission rate, abundance, and oxidation products in the atmosphere, *Atmos Chem Phys*, 9, 2061-2074, 2009.

Bouvier-Brown, N. C.: Quantifying reactive biogenic volatile organic compounds: Implications for gas-and particle-phase atmospheric chemistry, ProQuest, University of California, Berkeley, CA, 2008.

Bursey, M. M., and McLafferty, F. W.: Rearrangements and “Flat-Topped Metastable Ions” in the Mass Spectra of Substituted Nitrobenzenes¹, *J Am Chem Soc*, 88, 5023-5025, 10.1021/ja00973a047, 1966.

Bursey, M. M.: Influence of steric inhibition of resonance on ion intensities in mass spectra, *J Am Chem Soc*, 91, 1861-1862, 10.1021/ja01035a053, 1969.

Cahill, T. M., Seaman, V. Y., Charles, M. J., Holzinger, R., and Goldstein, A. H.: Secondary organic aerosols formed from oxidation of biogenic volatile organic compounds in the Sierra Nevada Mountains of California, *Journal of geophysical research*, 111, D16312, doi: 10.1029/2006JD007178, 2006.

Calvert, J. G., Atkinson, R., Kerr, J., Madronich, S., Moortgat, G., Wallington, T. J., and Yarwood, G.: The mechanisms of atmospheric oxidation of the alkenes, Oxford University Press New York, 2000.

Calvert, J. G., Atkinson, R., Becker, K. H., Kamens, R. M., Seinfeld, J. H., Wallington, T. J., and Yarwood, G.: The mechanisms of atmospheric oxidation of aromatic hydrocarbons, Oxford University Press New York, 2002.

Camredon, M., Aumont, B., Lee-Taylor, J., and Madronich, S.: The SOA/VOC/NO_x system: an explicit model of secondary organic aerosol formation, *Atmos. Chem. Phys.*, 7, 5599-5610, 10.5194/acp-7-5599-2007, 2007.

Carlton, A., Wiedinmyer, C., and Kroll, J.: A review of Secondary Organic Aerosol (SOA) formation from isoprene, *Atmos Chem Phys*, 9, 4987-5005, 2009.

Carter, W., Atkinson, R., Winer, A., and Pitts, J.: Evidence for chamber-dependent radical sources: Impact on kinetic computer models for air pollution, *Int J Chem Kinet*, 13, 735-740, 1981.

Carter, W., Atkinson, R., Winer, A., and Pitts, J.: Experimental investigation of chamber-dependent radical sources, *Int J Chem Kinet*, 14, 1071-1103, 1982.

Cvetanovic, R.: Chemical kinetic studies of atmospheric interest, 12th International Symposium on Free Radicals, 4-9 January, Laguna Beach, CA, 1976,

Davidson, C. I., Phalen, R. F., and Solomon, P. A.: Airborne particulate matter and human health: A review, *Aerosol Science and Technology*, 39, 737-749, 2005.

De Vincenzi, M., Silano, M., Maialetti, F., and Scazzocchio, B.: Constituents of aromatic plants: II. Estragole, *Fitoterapia*, 71, 725-729, 2000.

Donahue, N., Robinson, A., Stanier, C., and Pandis, S.: Coupled partitioning, dilution, and chemical aging of semivolatile organics, *Environmental science & technology*, 40, 2635-2643, 2006a.

Donahue, N., Kroll, J., Pandis, S., and Robinson, A.: A two-dimensional volatility basis set—Part 2: Diagnostics of organic-aerosol evolution, *Atmos Chem Phys*, 12, 615-634, 2012.

Donahue, N., Chuang, W., Ortega, I. K., Riipinen, I., Riccobono, F., Schobesberger, S., Dommen, J., Kulmala, M., Worsnop, D., and Vehkamäki, H.: How Do Organic Vapors Contribute to New-Particle Formation?, *Faraday discussions.*, 165, 1-13, doi: 10.1039/c3fd00046j, 2013.

Donahue, N. M., Robinson, A. L., Stanier, C. O., and Pandis, S. N.: Coupled Partitioning, Dilution, and Chemical Aging of Semivolatile Organics, *Environmental science & technology*, 40, 2635-2643, 10.1021/es052297c, 2006b.

Food and Agriculture Organization of the United Nations: <http://faostat3.fao.org/faostat-gateway/>, (last access: 11 August 2013), 2012.

Fitzherbert, E. B., Struebig, M. J., Morel, A., Danielsen, F., Brühl, C. A., Donald, P. F., and Phalan, B.: How will oil palm expansion affect biodiversity?, *Trends in Ecology & Evolution*, 23, 538-545, 10.1016/j.tree.2008.06.012, 2008.

Forstner, H. J., Flagan, R. C., and Seinfeld, J. H.: Secondary organic aerosol from the photooxidation of aromatic hydrocarbons: Molecular composition, *Environmental science & technology*, 31, 1345-1358, 1997.

Fu, X., Zhang, Y., Shi, S., Gao, F., Wen, D., Li, W., Liao, Y., and Liu, H.: Fragmentation study of hexanitrostilbene by ion trap multiple mass spectrometry and analysis by liquid chromatography/mass spectrometry, *Rapid Communications in Mass Spectrometry*, 20, 2906-2914, 2006.

Fuchs, H., Bohn, B., Hofzumahaus, A., Holland, F., Lu, K. D., Nehr, S., Rohrer, F., and Wahner, A.: Detection of HO₂ by laser-induced fluorescence: calibration and interferences from RO₂ radicals, *Atmos. Meas. Tech.*, 4, 1209-1225, 10.5194/amt-4-1209-2011, 2011.

Gai, Y., Wang, W., Ge, M., Kjaergaard, H. G., Jørgensen, S., and Du, L.: Methyl chavicol reactions with ozone, OH and NO₃ radicals: Rate constants and gas-phase products, *Atmospheric Environment*, 77, 696-702, <http://dx.doi.org/10.1016/j.atmosenv.2013.05.041>, 2013.

Goldstein, A. H., and Galbally, I. E.: Known and unexplored organic constituents in the earth's atmosphere, *Environmental science & technology*, 41, 1514-1521, 2007.

Guenther, A., Hewitt, C. N., Erickson, D., Fall, R., Geron, C., Graedel, T., Harley, P., Klinger, L., Lerdau, M., and McKay, W.: A global model of natural volatile organic compound emissions, *Journal of geophysical research*, 100, 8873-8892, 1995.

Guenther, A., Geron, C., Pierce, T., Lamb, B., Harley, P., and Fall, R.: Natural emissions of non-methane volatile organic compounds, carbon monoxide, and oxides of nitrogen from North America, *Atmospheric Environment*, 34, 2205-2230, 2000.

M. Hallquist, J. C. Wenger, U. Baltensperger, Y. Rudich, D. Simpson, M. Claeys, J. Dommen, N. M. Donahue, C. George, A. H. Goldstein, J. F. Hamilton, H. Herrmann, T. Hoffmann, Y. Iinuma, M. Jang, M. E. Jenkin, J. L. Jimenez, A. Kiendler-Scharr, W. Maenhaut, G. McFiggans, Th. F. Mentel, A. Monod, A. S. H. Prévôt, J. H. Seinfeld, J. D. Surratt, R. Szmigielski, and Wildt, J.: The formation, properties and impact of secondary organic aerosol: current and emerging issues, *Atmos Chem Phys*, 9, 5155-5236, 2009.

Hayen, H., Jachmann, N., Vogel, M., and Karst, U.: LC-Electron capture APCI-MS for the determination of nitroaromatic compounds, *Analyst*, 127, 1027-1030, 2002.

Healy, R. M., Temime, B., Kuprovskite, K., and Wenger, J. C.: Effect of relative humidity on gas/particle partitioning and aerosol mass yield in the photooxidation of p-xylene, *Environmental science & technology*, 43, 1884-1889, 2009.

Hewitt, C. N., MacKenzie, A. R., Di Carlo, P., Di Marco, C. F., Dorsey, J. R., Evans, M., Fowler, D., Gallagher, M. W., Hopkins, J. R., Jones, C. E., Langford, B., Lee, J. D., Lewis, A. C., Lim, S. F., McQuaid, J., Misztal, P., Moller, S. J., Monks, P. S., Nemitz, E., Oram, D. E., Owen, S. M., Phillips, G. J., Pugh, T. A. M., Pyle, J. A., Reeves, C. E., Ryder, J., Siong, J., Skiba, U., and Stewart, D. J.: Nitrogen management is essential to prevent tropical oil palm plantations from causing ground-level ozone pollution, *Proceedings of the National Academy of Sciences*, 106, 18447-18451, 10.1073/pnas.0907541106, 2009.

Holčápek, M., Lísa, M., Volná, K., Almonasy, N., and Přikryl, J.: Occurrence of radical molecular ions in atmospheric pressure chemical ionization mass spectra of heterocyclic compounds, *J Mass Spectrom*, 42, 1645-1648, 10.1002/jms.1318, 2007.

Holčápek, M., Jirásko, R., and Lísa, M.: Basic rules for the interpretation of atmospheric pressure ionization mass spectra of small molecules, *Journal of Chromatography A*, 1217, 3908-3921, 2010.

Holzinger, R., Lee, A., Paw, K., and Goldstein, U.: Observations of oxidation products above a forest imply biogenic emissions of very reactive compounds, *Atmos Chem Phys*, 5, 67-75, 2005.

Holzinger, R., Kasper-Giebl, A., Staudinger, M., Schauer, G., and Röckmann, T.: Analysis of the chemical composition of organic aerosol at the Mt. Sonnblick observatory using a novel high mass resolution thermal-desorption proton-transfer-reaction mass-spectrometer (hr-TD-PTR-MS), *Atmos Chem Phys*, 10, 10111-10128, 2010.

Howard, J. A., and Ingold, K. U.: Self-reaction of sec-butylperoxy radicals. Confirmation of the Russell mechanism, *J Am Chem Soc*, 90, 1056-1058, 10.1021/ja01006a037, 1968.

Huang, M., Hao, L., Gu, X., Hu, C., Zhao, W., Wang, Z., Fang, L., and Zhang, W.: Effects of inorganic seed aerosols on the growth and chemical composition of secondary organic aerosol formed from OH-initiated oxidation of toluene, *J Atmos Chem*, 70, 151-164, 10.1007/s10874-013-9262-9, 2013.

Inuma, Y., Böge, O., Keywood, M., Gnauk, T., and Herrmann, H.: Diaterebic Acid Acetate and Diaterpenylic Acid Acetate: Atmospheric Tracers for Secondary Organic Aerosol Formation from 1,8-Cineole Oxidation, *Environmental science & technology*, 43, 280-285, 10.1021/es802141v, 2008.

Jacobson, M., Hansson, H., Noone, K., and Charlson, R.: Organic atmospheric aerosols: Review and state of the science, *REVIEWS OF GEOPHYSICS-RICHMOND VIRGINIA THEN WASHINGTON-*, 38, 267-294, 2000.

Jimenez, J. L., Canagaratna, M. R., Donahue, N. M., Prevot, A. S. H., Zhang, Q., Kroll, J. H., DeCarlo, P. F., Allan, J. D., Coe, H., Ng, N. L., Aiken, A. C., Docherty, K. S., Ulbrich, I. M., Grieshop, A. P., Robinson, A. L., Duplissy, J., Smith, J. D., Wilson, K. R., Lanz, V. A., Hueglin, C., Sun, Y. L., Tian, J., Laaksonen, A., Raatikainen, T., Rautiainen, J., Vaattovaara, P., Ehn, M., Kulmala, M., Tomlinson, J. M., Collins, D. R., Cubison, M. J., E., Dunlea, J.,

Huffman, J. A., Onasch, T. B., Alfarra, M. R., Williams, P. I., Bower, K., Kondo, Y., Schneider, J., Drewnick, F., Borrmann, S., Weimer, S., Demerjian, K., Salcedo, D., Cottrell, L., Griffin, R., Takami, A., Miyoshi, T., Hatakeyama, S., Shimono, A., Sun, J. Y., Zhang, Y. M., Dzepina, K., Kimmel, J. R., Sueper, D., Jayne, J. T., Herndon, S. C., Trimborn, A. M., Williams, L. R., Wood, E. C., Middlebrook, A. M., Kolb, C. E., Baltensperger, U., and Worsnop, D. R.: Evolution of Organic Aerosols in the Atmosphere, *Science*, 326, 1525-1529, 10.1126/science.1180353, 2009.

Kebarle, P., and Verkerk, U. H.: Electrospray: From ions in solution to ions in the gas phase, what we know now, *Mass Spectrometry Reviews*, 28, 898-917, 10.1002/mas.20247, 2009.

Khan, S., Zhang, Q., and Broadbelt, L.: Automated mechanism generation. Part 1: mechanism development and rate constant estimation for VOC chemistry in the atmosphere, *J Atmos Chem*, 63, 125-156, 10.1007/s10874-010-9164-z, 2009.

Kind, T., and Fiehn, O.: Metabolomic database annotations via query of elemental compositions: mass accuracy is insufficient even at less than 1 ppm, *BMC bioinformatics*, 7, 234, doi: 10.1186/1471-2105-7-234, 2006.

Klotz, B., Sørensen, S., Barnes, I., Becker, K. H., Etzkorn, T., Volkamer, R., Platt, U., Wirtz, K., and Martín-Reviejo, M.: Atmospheric oxidation of toluene in a large-volume outdoor photoreactor: In situ determination of ring-retaining product yields, *The Journal of Physical Chemistry A*, 102, 10289-10299, 1998.

Kroll, J. H., Chan, A. W. H., Ng, N. L., Flagan, R. C., and Seinfeld, J. H.: Reactions of Semivolatile Organics and Their Effects on Secondary Organic Aerosol Formation, *Environmental science & technology*, 41, 3545-3550, 10.1021/es062059x, 2007.

Kroll, J. H., and Seinfeld, J. H.: Chemistry of secondary organic aerosol: Formation and evolution of low-volatility organics in the atmosphere, *Atmospheric Environment*, 42, 3593-3624, <http://dx.doi.org/10.1016/j.atmosenv.2008.01.003>, 2008.

Lee, A., Goldstein, A. H., Keywood, M. D., Gao, S., Varutbangkul, V., Bahreini, R., Ng, N. L., Flagan, R. C., and Seinfeld, J. H.: Gas-phase products and secondary aerosol yields from the ozonolysis of ten different terpenes, *J. Geophys. Res.*, 111, D07302, doi: 10.1029/2005JD006437, 2006a.

Lee, A., Goldstein, A. H., Kroll, J. H., Ng, N. L., Varutbangkul, V., Flagan, R. C., and Seinfeld, J. H.: Gas-phase products and secondary aerosol yields from the photooxidation of 16 different terpenes, *J. Geophys. Res.*, 111, D17305, doi: 10.1029/2006JD007050, 2006b.

Lu, Z., Hao, J., Takekawa, H., Hu, L., and Li, J.: Effect of high concentrations of inorganic seed aerosols on secondary organic aerosol formation in the m-xylene/NO_x photooxidation system, *Atmospheric Environment*, 43, 897-904, 2009.

MacKenzie, A. R., Langford, B., Pugh, T. A. M., Robinson, N., Misztal, P. K., Heard, D. E., Lee, J. D., Lewis, A. C., Jones, C. E., Hopkins, J. R., Phillips, G., Monks, P. S., Karunaharan, A., Hornsby, K. E., Nicolas-Perea, V., Coe, H., Gabey, A. M., Gallagher, M. W., Whalley, L. K., Edwards, P. M., Evans, M. J., Stone, D., Ingham, T., Commane, R., Furneaux, K. L., McQuaid, J. B., Nemitz, E., Seng, Y. K., Fowler, D., Pyle, J. A., and Hewitt, C. N.: The atmospheric chemistry of trace gases and particulate matter emitted by different land uses in Borneo, *Philosophical Transactions of the Royal Society B: Biological Sciences*, 366, 3177-3195, 10.1098/rstb.2011.0053, 2011.

Madronich, S., and Calvert, J. G.: Permutation reactions of organic peroxy radicals in the troposphere, *Journal of Geophysical Research: Atmospheres*, 95, 5697-5715, 10.1029/JD095iD05p05697, 1990.

March, J.: *Advanced organic chemistry: reactions, mechanisms, and structure*, John Wiley & Sons, New York, 1992.

Mirov, N. T.: *Composition of gum turpentines of pines*, USDA forest service, Technical Bulletin No. 1239, 158 pp, 1961.

Misztal, P. K., Owen, S., Guenther, A. B., Rasmussen, R., Geron, C., Harley, P., Phillips, G., Ryan, A., Edwards, D. P., and Hewitt, C. N.: Large estragole fluxes from oil palms in Borneo, *Atmos. Chem. Phys.*, 10, 4343-4358, 2010.

Official Portal Of Malaysian Palm Oil Board: <http://bepi.mpob.gov.my/>, (last access: 11 April 2013), 2012.

Nannoolal, Y., Rarey, J., Ramjugernath, D., and Cordes, W.: Estimation of pure component properties: Part 1. Estimation of the normal boiling point of non-electrolyte organic compounds via group contributions and group interactions, *Fluid Phase Equilibria*, 226, 45-63, <http://dx.doi.org/10.1016/j.fluid.2004.09.001>, 2004.

Nannoolal, Y., Rarey, J., and Ramjugernath, D.: Estimation of pure component properties: Part 3. Estimation of the vapor pressure of non-electrolyte organic compounds via group contributions and group interactions, *Fluid Phase Equilibria*, 269, 117-133, 2008.

Neeb, P., Horie, O., and Moortgat, G. K.: Gas-phase ozonolysis of ethene in the presence of hydroxylic compounds, *Int J Chem Kinet*, 28, 721-730, 10.1002/(sici)1097-4601(1996)28:10<721::aid-kin2>3.0.co;2-p, 1996.

O'Neal, H. E., and Blumstein, C.: A new mechanism for gas phase ozone–olefin reactions, *Int J Chem Kinet*, 5, 397-413, 1973.

Odum, J. R., Hoffmann, T., Bowman, F., Collins, D., Flagan, R. C., and Seinfeld, J. H.: Gas/Particle Partitioning and Secondary Organic Aerosol Yields, *Environmental science & technology*, 30, 2580-2585, 10.1021/es950943+, 1996.

Orlando, J. J., Tyndall, G. S., and Wallington, T. J.: The atmospheric chemistry of alkoxy radicals, *Chemical reviews*, 103, 4657-4690, 2003.

Orsini, D. A., Ma, Y., Sullivan, A., Sierau, B., Baumann, K., and Weber, R. J.: Refinements to the particle-into-liquid sampler (PILS) for ground and airborne measurements of water soluble aerosol composition, *Atmospheric Environment*, 37, 1243-1259, 2003.

Orzechowska, G. E., and Paulson, S. E.: Photochemical Sources of Organic Acids. 1. Reaction of Ozone with Isoprene, Propene, and 2-Butenes under Dry and Humid Conditions Using SPME, *The Journal of Physical Chemistry A*, 109, 5358-5365, 10.1021/jp050166s, 2005.

Pankow, J. F.: An absorption model of the gas/aerosol partitioning involved in the formation of secondary organic aerosol, *Atmospheric Environment*, 28, 189-193, 1994a.

Pankow, J. F.: An absorption model of gas/particle partitioning of organic compounds in the atmosphere, *Atmospheric Environment*, 28, 185-188, 1994b.

Peeters, J., Boullart, W., Pultau, V., Vandenberg, S., and Vereecken, L.: Structure–Activity Relationship for the Addition of OH to (Poly)alkenes: Site-Specific and Total Rate Constants, *The Journal of Physical Chemistry A*, 111, 1618-1631, 10.1021/jp066973o, 2007.

Pellegrin, V.: Molecular formulas of organic compounds: the nitrogen rule and degree of unsaturation, *Journal of Chemical Education*, 60, 626, doi: 10.1021/ed060p626, 1983.

Pitts, J. N., Biermann, H. W., Atkinson, R., and Winer, A. M.: Atmospheric implications of simultaneous nighttime measurements of NO₃ radicals and HONO, *Geophysical Research Letters*, 11, 557-560, 10.1029/GL011i005p00557, 1984.

Pöschl, U.: Atmospheric Aerosols: Composition, Transformation, Climate and Health Effects, *Angewandte Chemie International Edition*, 44, 7520-7540, 10.1002/anie.200501122, 2005.

Rickard, A. R., Wyche, K. P., Metzger, A., Monks, P. S., Ellis, A. M., Dommen, J., Baltensperger, U., Jenkin, M. E., and Pilling, M. J.: Gas phase precursors to anthropogenic secondary organic aerosol: Using the Master Chemical Mechanism to probe detailed observations of 1,3,5-trimethylbenzene photo-oxidation, *Atmospheric Environment*, 44, 5423-5433, <http://dx.doi.org/10.1016/j.atmosenv.2009.09.043>, 2010.

Sakamaki, F., Hatakeyama, S., and Akimoto, H.: Formation of nitrous acid and nitric oxide in the heterogeneous dark reaction of nitrogen dioxide and water vapor in a smog chamber, *Int J Chem Kinet*, 15, 1013-1029, 10.1002/kin.550151006, 1983.

Schade, G. W., and Goldstein, A. H.: Fluxes of oxygenated volatile organic compounds from a ponderosa pine plantation, *Journal of geophysical research*, 106, 3111-3123, 2001.

Schmidt, A.-C., Herzsuh, R., Matysik, F.-M., and Engewald, W.: Investigation of the ionisation and fragmentation behaviour of different nitroaromatic compounds occurring as polar metabolites of explosives using electrospray ionisation tandem mass spectrometry, *Rapid Communications in Mass Spectrometry*, 20, 2293-2302, 10.1002/rcm.2591, 2006.

Singh, H., Chen, Y., Tabazadeh, A., Fukui, Y., Bey, I., Yantosca, R., Jacob, D., Arnold, F., Wohlfrom, K., Atlas, E., Flocke, F., Blake, D., Blake, N., Heikes, B., Snow, J., Talbot, R., Gregory, G., Sachse, G., Vay, S., and Kondo, Y.: Distribution and fate of selected oxygenated organic species in the troposphere and lower stratosphere over the Atlantic, *Journal of Geophysical Research: Atmospheres*, 105, 3795-3805, 10.1029/1999jd900779, 2000.

Solomon, S., Qin, D., Manning, M., Chen, Z., Marquis, M., Averyt, K., Tignor, M., and Miller, H.: *Climate change 2007: the physical science basis: working Group I contribution to the fourth assessment report of the IPCC*, Cambridge University Press: Cambridge, 2007.

Song, C., Na, K., and Cocker, D. R.: Impact of the Hydrocarbon to NO_x Ratio on Secondary Organic Aerosol Formation, *Environmental science & technology*, 39, 3143-3149, 10.1021/es0493244, 2005.

Southwell, I. A., Russell, M. F., Smith, R. L., and Vinnicombe, A.: *Ochrosperma lineare*, a new source of methyl chavicol, *Journal of Essential Oil Research*, 15, 329-330, 2003.

Spada, N., Fujii, E., and Cahill, T. M.: Diurnal Cycles of Acrolein and Other Small Aldehydes in Regions Impacted by Vehicle Emissions, *Environmental science & technology*, 42, 7084-7090, 10.1021/es801656e, 2008.

Steiner, A. L., Cohen, R. C., Harley, R. A., Tonse, S., Millet, D. B., Schade, G. W., and Goldstein, A. H.: VOC reactivity in central California: comparing an air quality model to ground-based measurements, *Atmos. Chem. Phys.*, 8, 351-368, 10.5194/acp-8-351-2008, 2008.

Stockwell, W. R., Middleton, P., Chang, J. S., and Tang, X.: The second generation regional acid deposition model chemical mechanism for regional air quality modeling, *Journal of Geophysical Research*, 95, 16343-16316,16367, 1990.

Svensson, R., Ljungström, E., and Lindqvist, O.: Kinetics of the reaction between nitrogen dioxide and water vapour, *Atmospheric Environment (1967)*, 21, 1529-1539, 1987.

Taipale, R., Rantala, P., Kajos, M., Patokoski, J., Ruuskanen, T., Aalto, J., Kolari, P., Bäck, J., Hari, P., Kulmala, M., and Rinne, J.: Oxygenated VOC and monoterpene emissions from a boreal coniferous forest, *EGU General Assembly Conference Abstracts*, 9735, 2012.

United States Department of Agriculture, *Global Crop Production Analysis*: <http://www.pecad.fas.usda.gov>, access: 04/11/2013, 2013.

Varutbangkul, V., Brechtel, F., Bahreini, R., Ng, N., Keywood, M., Kroll, J., Flagan, R., Seinfeld, J., Lee, A., and Goldstein, A.: Hygroscopicity of secondary organic aerosols formed by oxidation of cycloalkenes, monoterpenes, sesquiterpenes, and related compounds, *Atmos Chem Phys*, 6, 2367-2388, 2006.

Werker, E., Putievsky, E., Ravid, U., Dudai, N., and Katzir, I.: Glandular Hairs, Secretary Cavities, and the Essential Oil in the Leaves of Tarragon (*Artemisia dracunculus* L.), *Journal of Herbs, Spices & Medicinal Plants*, 2, 19-32, 1994.

Wiedinmyer, C., Guenther, A., Harley, P., Hewitt, N., Geron, C., Artaxo, P., Steinbrecher, R., and Rasmussen, R.: Global Organic Emissions from Vegetation, in: Emissions of Atmospheric Trace Compounds, edited by: Granier, C., Artaxo, P., and Reeves, C., Advances in Global Change Research, Springer Netherlands, 115-170, 2004.

Yinon, J., McClellan, J. E., and Yost, R. A.: Electrospray ionization tandem mass spectrometry collision-induced dissociation study of explosives in an ion trap mass spectrometer, *Rapid Communications in Mass Spectrometry*, 11, 1961-1970, 10.1002/(sici)1097-0231(199712)11:18<1961::aid-rcm99>3.0.co;2-k, 1997.

Zhao, X., and Yinon, J.: Identification of nitrate ester explosives by liquid chromatography–electrospray ionization and atmospheric pressure chemical ionization mass spectrometry, *Journal of Chromatography A*, 977, 59-68, [http://dx.doi.org/10.1016/S0021-9673\(02\)01349-3](http://dx.doi.org/10.1016/S0021-9673(02)01349-3), 2002.

Zhou, Y., Zhang, H., Parikh, H. M., Chen, E. H., Rattanavaraha, W., Rosen, E. P., Wang, W., and Kamens, R. M.: Secondary organic aerosol formation from xylenes and mixtures of toluene and xylenes in an atmospheric urban hydrocarbon mixture: Water and particle seed effects (II), *Atmospheric Environment*, 45, 3882-3890, <http://dx.doi.org/10.1016/j.atmosenv.2010.12.048>, 2011.

Ziemann, P. J., and Atkinson, R.: Kinetics, products, and mechanisms of secondary organic aerosol formation, *Chemical Society Reviews*, 41, 6582-6605, 10.1039/c2cs35122f, 2012.

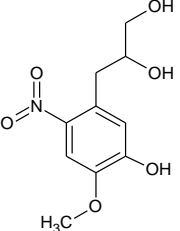
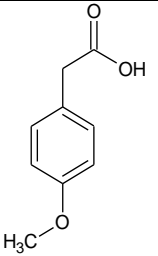
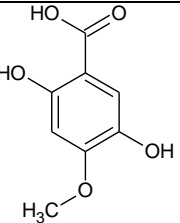
Zimmerman, P. R.: Testing of hydrocarbon emissions from vegetation, leaf litter and aquatic surfaces, and development of a methodology for compiling biogenic emission inventories[Final Report], Washington State University Pullman, Washington 99164, 1979.

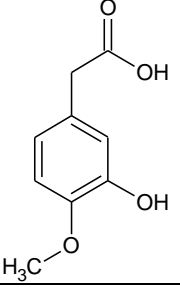
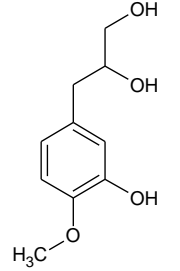
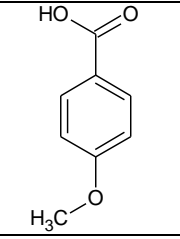
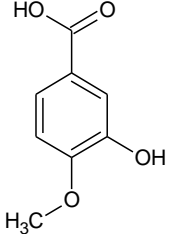
Table 1 – The initial experimental mixing ratios, temperature and relative humidity range for the experiments discussed.

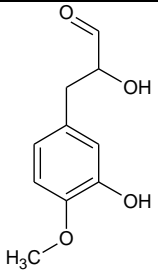
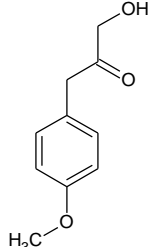
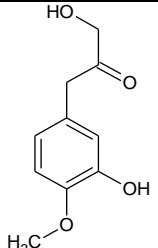
Exp.	Date	Exp. description	Initial mixing ratio ^a				Experimental range ^b	
			MC ^c	NO	NO ₂	O ₃	Temp	RH
			[ppbv]	[ppbv]	[ppbv]	[ppbv]	[K]	[%]
MC ₍₀₎	08.05.2012	Chamber background	0	0.3	0.7	0	294 – 312	0.7 – 4.7
MC _{low}	11.05.2012	Photosmog low concentration	212	38	8	2	298 - 308	0.9 – 14.7
MC _{high}	15.05.2012	Photosmog high concentration	460	92	3	5	297 - 306	2.1 -10.7

^a On the opening of the chamber covers. ^b From the opening to the closing of the chamber covers. ^c FTIR measurement.

Table 2 – The 10 structurally identified SOA compounds including; retention time (t_R), molecular formula (MF) identification and associated errors using HPLC-ITMS, FTICR-MS and HPLC-QTOFMS

Compound	IUPAC name	Compound structure	MC_{high}					
			MW [g mol ⁻¹]	t_R	FTICR-MS MF	FTICR-MS MF error [ppm]	HPLC- QTOFMS MF	HPLC- QTOFMS MF error [ppm]
1	3-(5-hydroxy-4-methoxy-2-nitrophenyl)propane-1,2-diol		243	22.2	C ₁₀ H ₁₃ NO ₆	0.6	C ₁₀ H ₁₃ NO ₆	-0.7
2	(4-methoxyphenyl)acetic acid**		166	28.1	C ₉ H ₁₀ O ₃	0.8	C ₉ H ₁₀ O ₃	1.2
3	2,5-dihydroxy-4-methoxybenzoic acid		184	10.2	^a		C ₈ H ₈ O ₅	48

4	(3-hydroxy-4-methoxyphenyl)acetic acid		182	16.1	C ₉ H ₁₀ O ₄	0.8	C ₉ H ₁₀ O ₄	-0.3
5	3-(3-hydroxy-4-methoxyphenyl)propane-1,2-diol		198	20.2	C ₁₀ H ₁₄ O ₄	0.9	C ₁₀ H ₁₄ O ₄	2.4
6	4-methoxybenzoic acid**		152	30.1	C ₈ H ₈ O ₃	0.3	C ₈ H ₈ O ₃	-1.4
7	3-hydroxy-4-methoxybenzoic acid		168	33.0	C ₈ H ₈ O ₄	0.7	C ₈ H ₈ O ₄	0.2

8	2-hydroxy-3-(3-hydroxy-4-methoxyphenyl)propanal		196	25.2	C ₁₀ H ₁₂ O ₄	1	C ₁₀ H ₁₂ O ₄	2.5
9	1-hydroxy-3-(4-methoxyphenyl)propan-2-one		180	27.6	^a		C ₁₀ H ₁₂ O ₃	-7.8
10	1-hydroxy-3-(3-hydroxy-4-methoxyphenyl)propan-2-one		196	19.8	C ₁₀ H ₁₂ O ₄ [*]	5	C ₁₀ H ₁₂ O ₄ [*]	9.4

^a = Deprotonated or protonated molecular species not observed in FTICR-MS spectra due to low concentration. * Identified as [M+Na]⁺, the Na adduct has been removed from molecular formula and molecular weight corrected. ** Compound structures confirmed using the commercially available standards.

Table 3 – Deprotonated molecular species fragmentation for compound 1, obtained from the use of the HPLC-ITMS² and the HPLC-QTOFMS²

MF	[M-H] ⁻	DBE	Fragment ion [m/z]	Fragment ion MF	DBE	Loss [Da]	Electron fragmentation	Fragment ion MF error [ppm]	MF Score [%]	Fragmentation shown
C ₁₀ H ₁₃ NO ₆	242	5	224	C₁₀H₁₀NO₅	6	18	EE	-2.1	100	Figure 2A
			182	C ₈ H ₈ NO ₄	5	(18+42) = 60	EE	-1	100	Figure 2B
			167	C ₇ H ₅ NO ₄	5*	(18+57) = 75	OE	8.8	100	Figure 2C
			137	C ₇ H ₅ O ₃	4**	105	OE	-19.2	100	Figure 2C

The highest intensity fragment ion is shown in bold. DBE = double bond equivalent. Electron fragmentation, EE = even electron, OE = odd electron. MF = molecular formula. *DBE was manually calculated, as automated DBE calculation is incorrect for radical fragment ions (DBE = 5.5 - 0.5 (for one ‘hydrogen atom deficiency’) = 5, see Pellegrin. (1983) for the calculation of DBE and DBE correction for radical ions). **DBE manually calculated, (DBE = 5 - 1 (for two ‘hydrogen atom deficiencies’) = 4).

Table 4 – Deprotonated molecular species fragmentation for compound 5, obtained from the use of the HPLC-ITMS² and the HPLC-QTOFMS²

MF	[M-H] ⁻	DBE	Fragment ion [<i>m/z</i>]	Fragment ion MF	DBE	Loss [Da]	Electron fragmentation	Fragment ion MF error [ppm]	MF Score [%]	Fragmentation shown
C ₁₀ H ₁₄ O ₄	197	4	179	C₁₀H₁₁O₃	5	18	EE	-19.3	100	Figure 3A
			137	C ₈ H ₉ O ₂	4	(18+42) = 60	EE	-0.5	100	Figure 3B
			123	C ₇ H ₇ O ₂	4	74	EE	-3.4	100	Figure 3C

The highest intensity fragment ion is shown in bold. DBE = double bond equivalent. Electron fragmentation, EE = even electron. MF = molecular formula.

Figure 1 – Temporal profiles of methyl chavicol, O₃, NO, NO₂ and SOA mass for MC_{low} and MC_{high} from the opening to the closing of the chamber housing. A = MC_{high}, (opening chamber housing = 8:42 am, closing of chamber housing 12:45 pm) B = MC_{low}, (opening chamber housing = 8:52 am, closing of chamber housing 12:42 pm). SOA mass is displayed on the secondary y-axis and corrected for wall loss and chamber dilution. Dashed lines display the PILS sample start time. PILS sample start time 10.43am in MC_{low} broken during transport.

Figure 2 – Proposed deprotonated molecular species fragmentation for compound 1 in negative ionisation mode. Dashed lines indicate the location of fragmentation.

Figure 3 – Proposed deprotonated molecular species fragmentation for compound 5 in negative ionisation mode. Dashed lines indicate the location of fragmentation.

Figure 4a – Mechanism of formation for the identified SOA compounds through the secondary β- hydroxyalkyl radical pathway, compounds 1, 5, 9 and 10, shown in brackets, refer to Table 2 for compound identification. See text for the explanation of the mechanism, letters refer to the text explanation. Boxes highlight identified SOA compounds.

Figure 4b – Mechanism of formation for the identified SOA compounds through the primary β-hydroxyalkyl radical pathway, compounds 1, 5 and 8, shown in brackets, refer to Table 2 for compound identification. See text for the explanation of the mechanism, letters refer to the text explanation. Boxes highlight identified SOA compounds.

Figure 5 – Oxygen to carbon ratio (O:C) and saturation concentration log C* (Donahue et al., 2006b) space to show the movement of the identified SOA compounds to lower volatilities upon oxidation in MC_{high}. Related generations of compounds are shown in the same colour. The change of shape but use of the same colour indicates a change in the SOA compound

structure through the reaction with $\cdot\text{OH}$ radicals or NO_2 . See legend for SOA compound identification and refer to Table 2. O:C/log C^* space with associated volatilities have been redrawn from Donahue et al. (2013) and Jimenez et al. (2009).

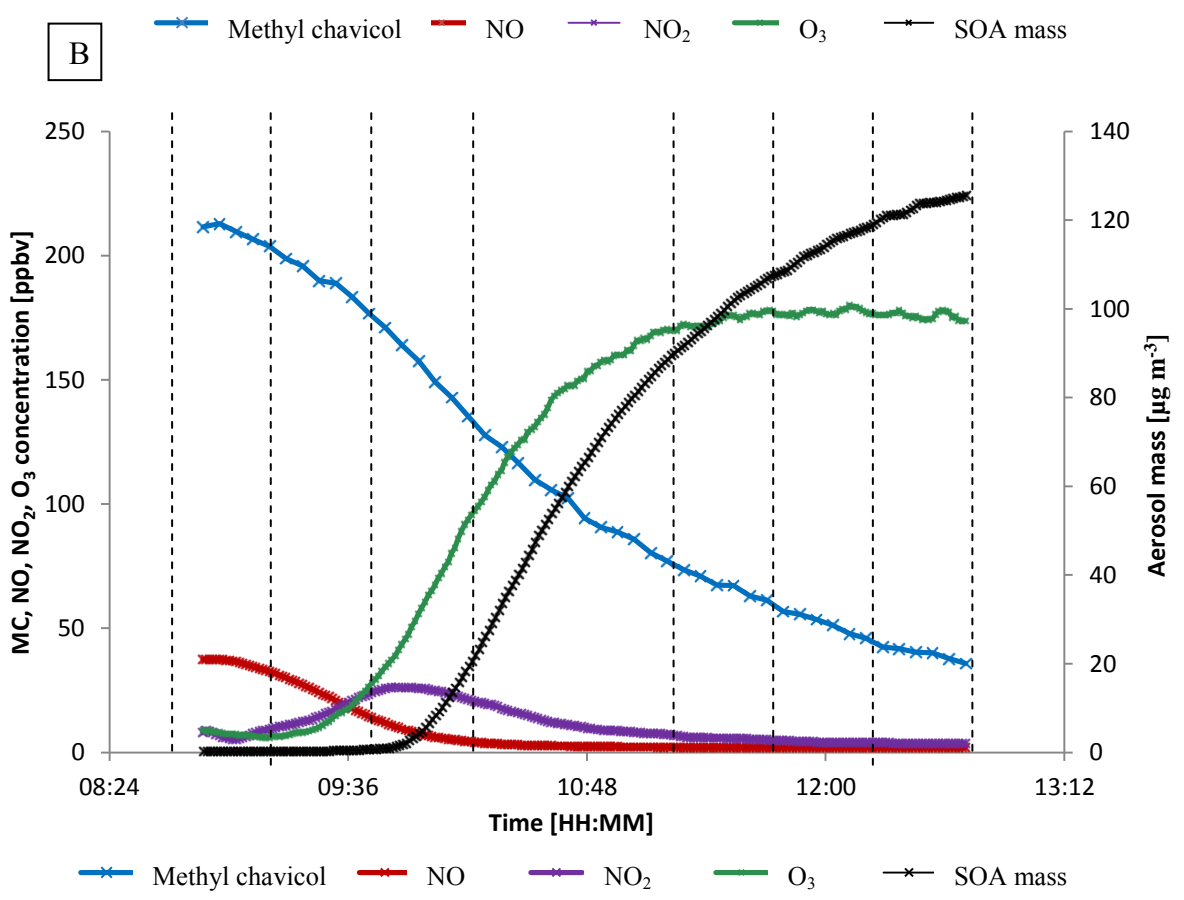
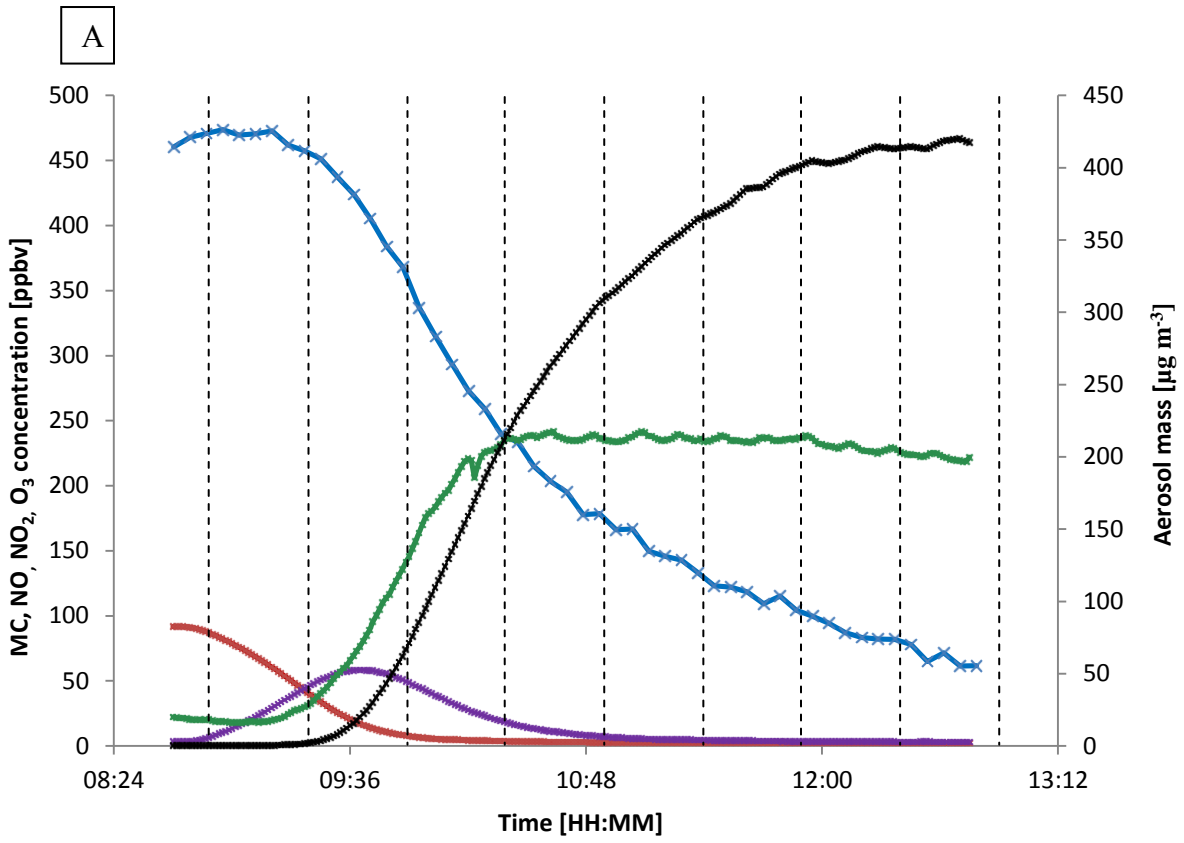


Figure 1

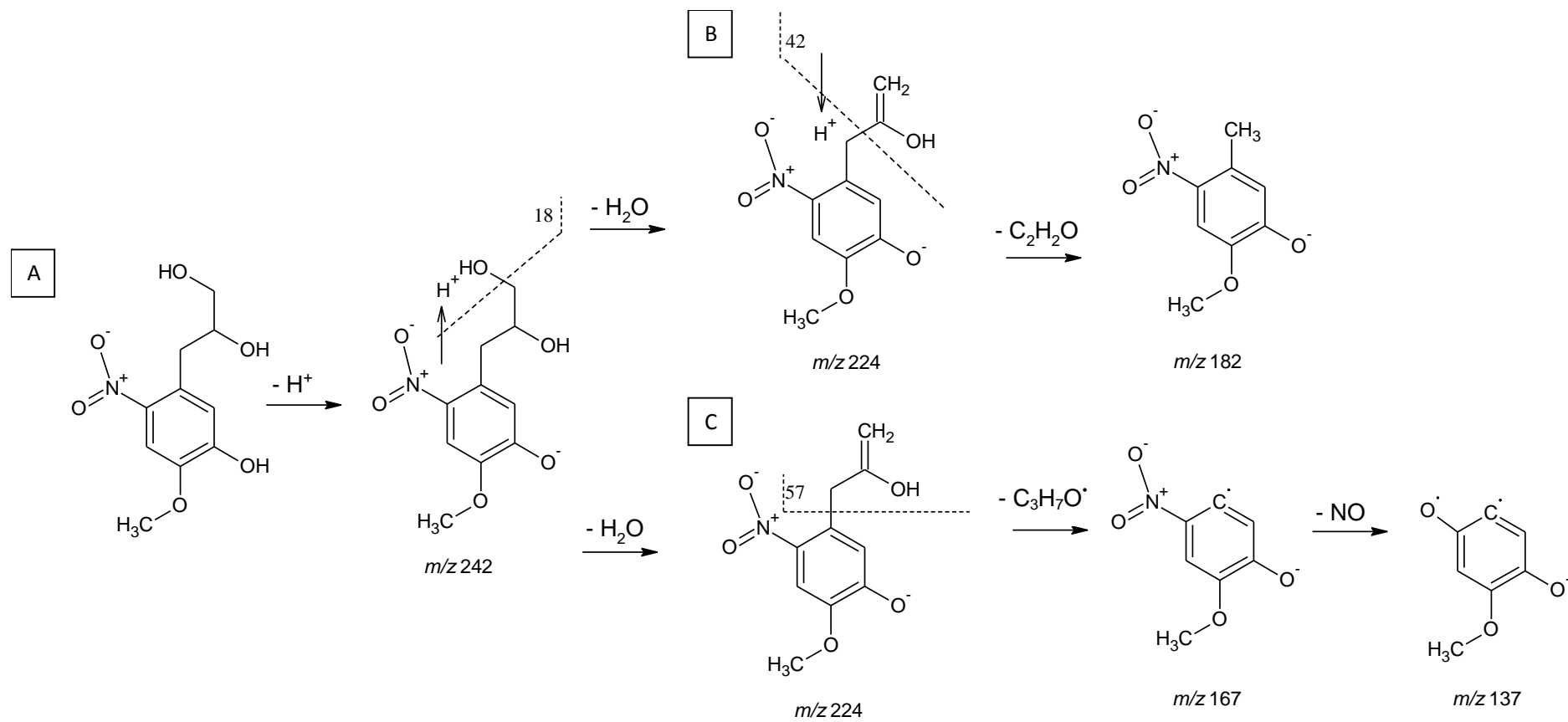


Figure 2

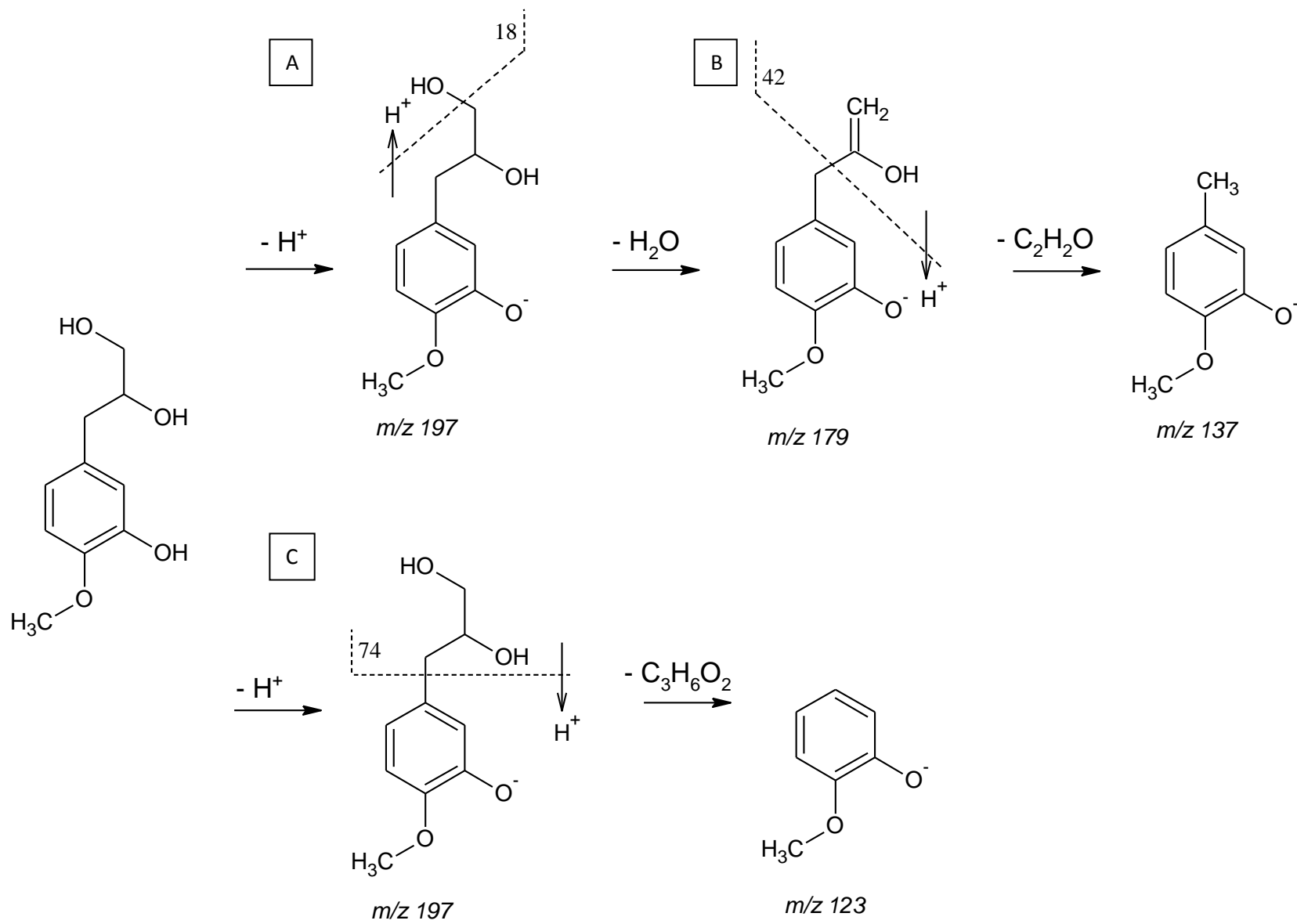


Figure 3

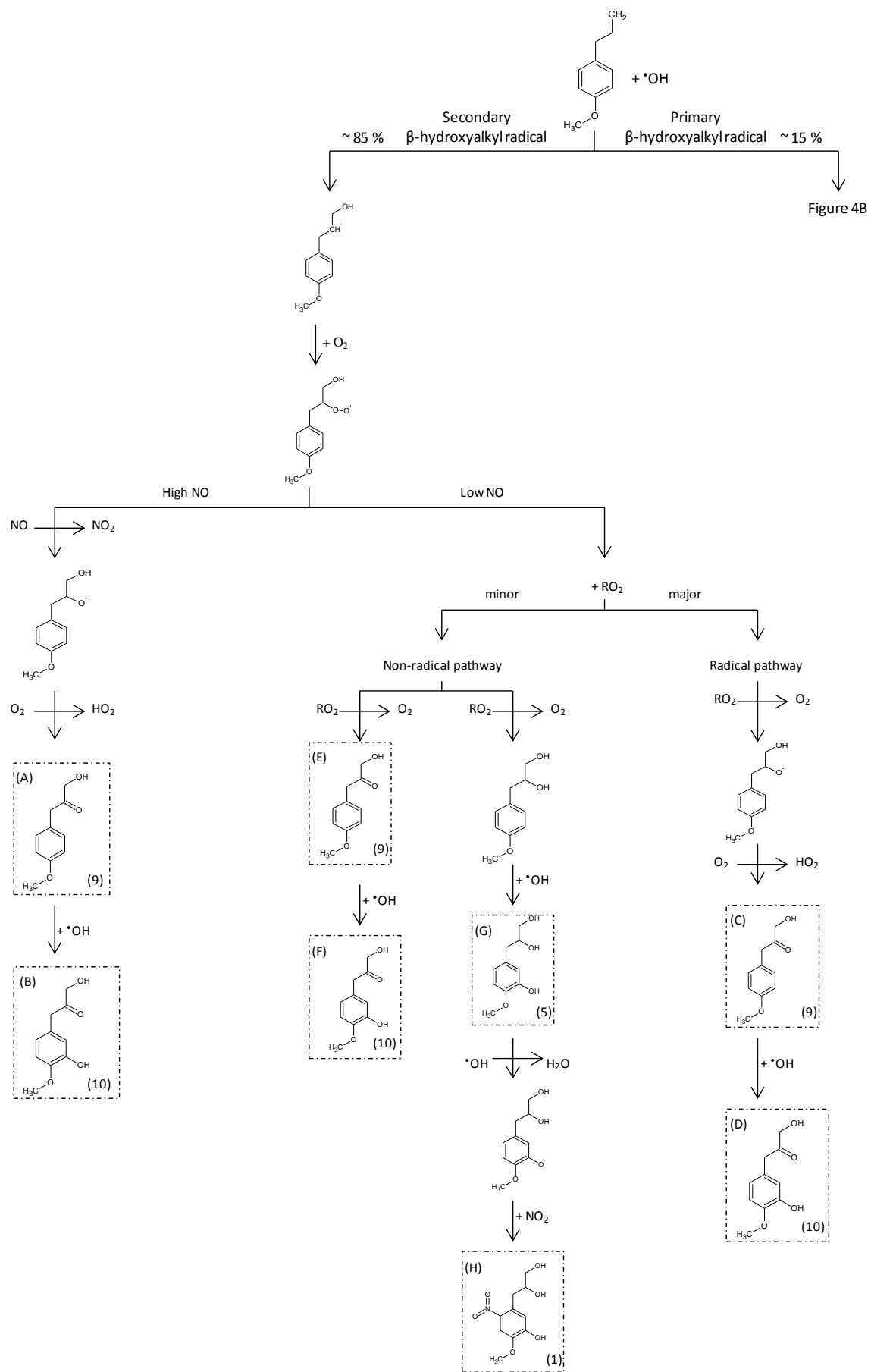


Figure 4a

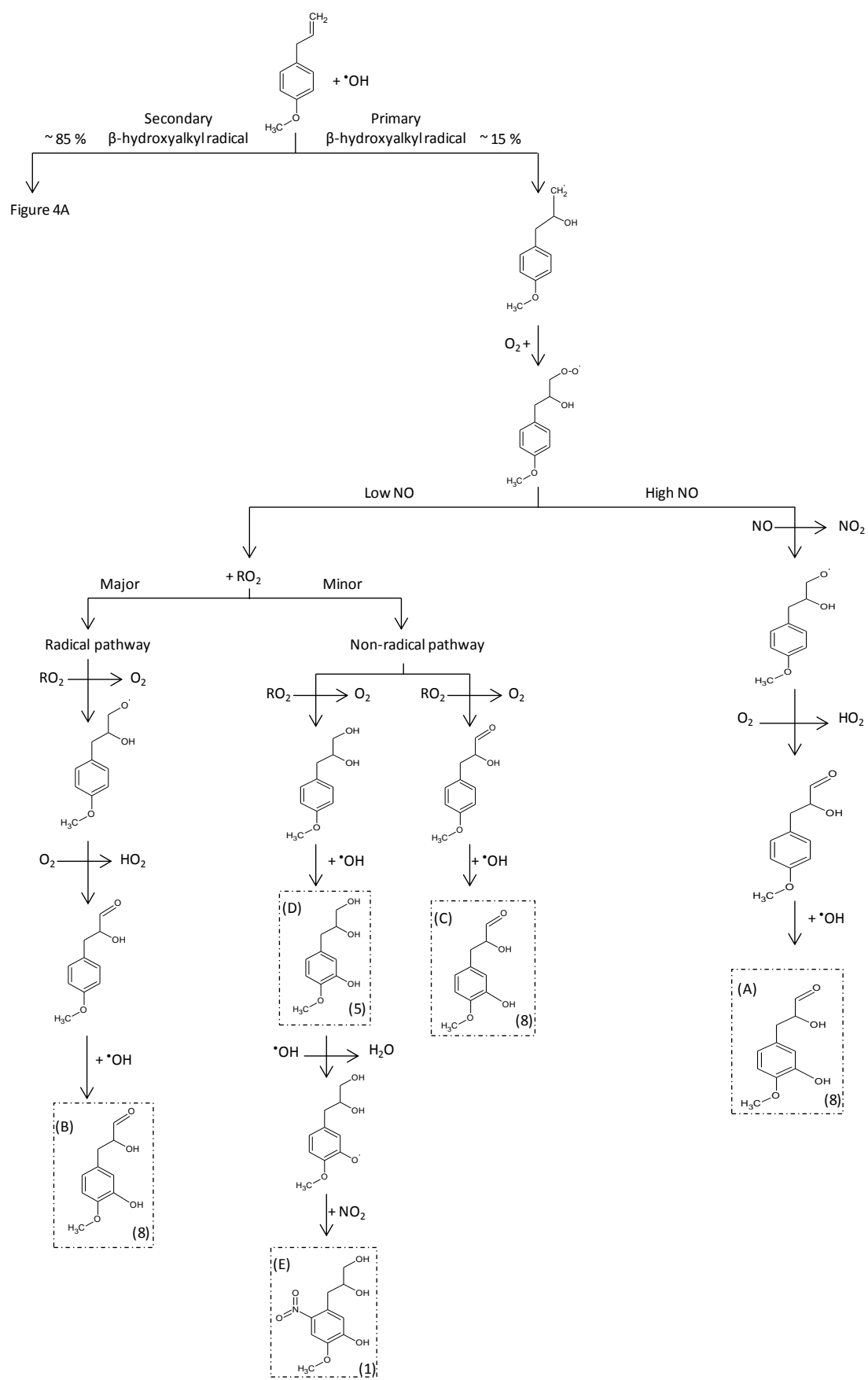


Figure 4b

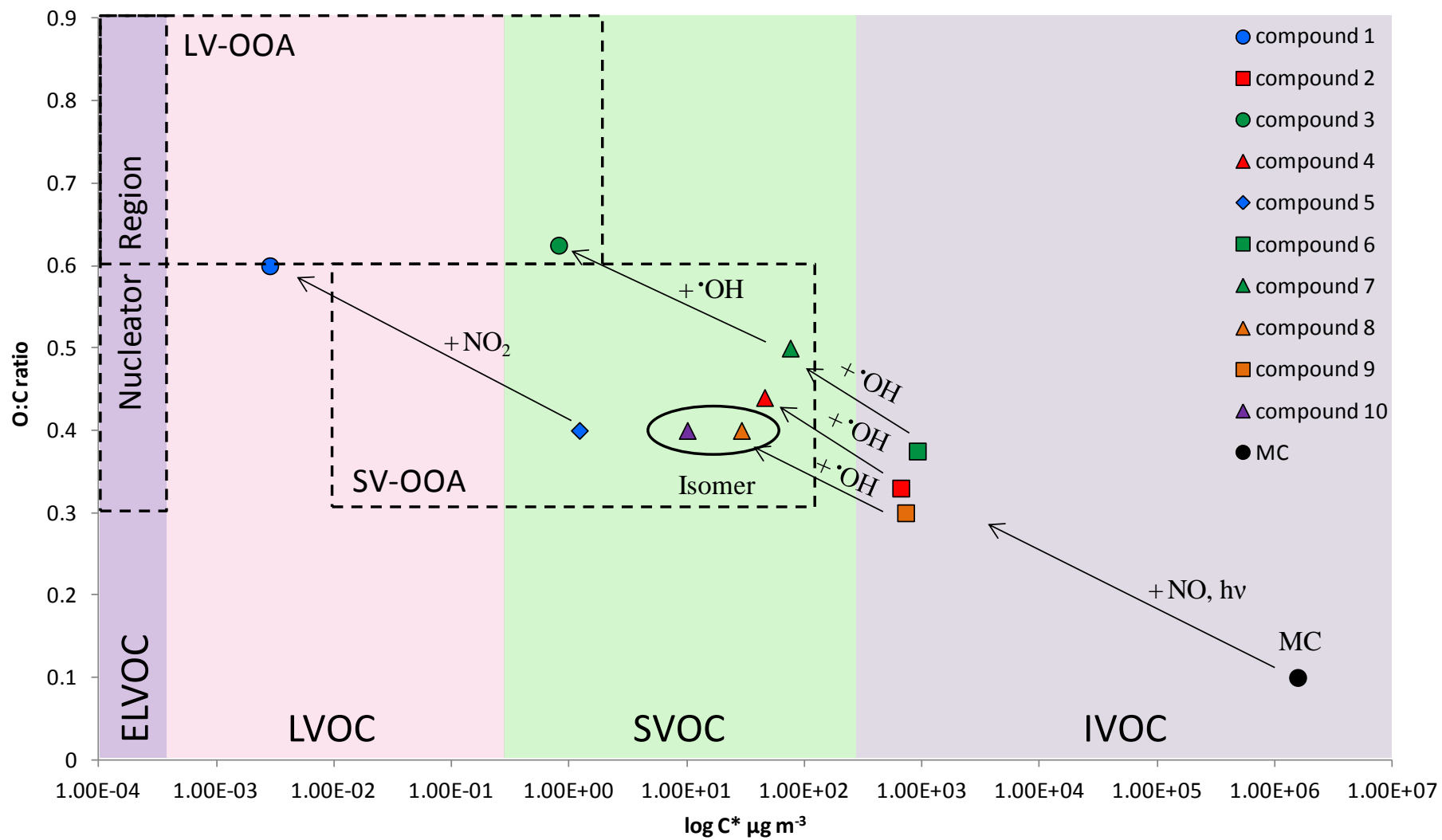


Figure 5